

Report

R-20-07

October 2020



Effects of water inflow to deposition hole during the installation phase

Peter Eriksson

SVENSK KÄRNBRÄNSLEHANTERING AB

SWEDISH NUCLEAR FUEL
AND WASTE MANAGEMENT CO

Box 3091, SE-169 03 Solna
Phone +46 8 459 84 00
skb.se

SVENSK KÄRNBRÄNSLEHANTERING

ISSN 1402-3091

SKB R-20-07

ID 1901398

October 2020

Effects of water inflow to deposition hole during the installation phase

Peter Eriksson, Svensk Kärnbränslehantering AB

Data in SKB's database can be changed for different reasons. Minor changes in SKB's database will not necessarily result in a revised report. Data revisions may also be presented as supplements, available at www.skb.se.

A pdf version of this document can be downloaded from www.skb.se.

© 2020 Svensk Kärnbränslehantering AB

Abstract

To understand how water flow behaves in bentonite pellet fillings and to better understand how the wetting pattern from point inflows in pellet fillings affect the swelling of buffer blocks models have been developed. The focus of the models has been to try and predict and understand the wetting and swelling of the buffer during the installation phase.

The work of water flow in pellet fillings is a continuation of the work that was done in the EBS task force (Eriksson 2019). The main new development has been to add a piping model. The water flow model together with the piping model gives very good agreement with experiments.

A new mechanical model has been developed and can reasonable well describe the swelling of the buffer block. However, the system is complex and for example slots between the blocks and cracking of the block need to be considered.

Even though the result is quite good the model needs to be optimized to be able to solve faster and be used on larger systems like a full deposition hole.

Sammanfattning

För att få en ökad förståelse för hur vatten beter sig i pellettfyllningar av bentonit och för att få en bättre förståelse hur bevättningsmönstret påverkar buffertblockens svällning har matematiska modeller utvecklats. Fokus för modellerna har varit på att försöka förstå och förutspå hur bevätningen och svällningen av bufferten beter sig under installationsfasen.

Arbetet med att modellera vattenflöde i pellettfyllningar är en fortsättning på arbetet som har gjorts i EBS Task force (Eriksson 2019). Den huvudsakliga utvecklingen som har gjorts är att lägga till en piping-modell. Vattenflödesmodellen tillsammans med piping-modellen ger resultat väldigt lika de försök som har gjorts.

En ny mekanisk modell utvecklats som relativt väl kan beskriva svällningen hos buffertblocken. Dock är systemet komplex och till exempel skarvarna mellan blocken och sprickbildning måste beaktas.

Även om resultatet från modelleringen är ganska bra så behöver modellerna optimeras och bli snabbare att lösa för att användas på större system som ett fullstort deponeringshål.

Contents

1	Introduction	7
2	Water flow in pellet fillings	9
3	Earlier tests	11
3.1	Test used to compare the model with	11
3.2	Water inflow in a 1 m section of a deposition hole (test 1)	11
3.3	Water inflow in a 1 m section of a deposition hole with extra weight (test 2)	13
	3.3.1 About the test	13
	3.3.2 Setup	13
	3.3.3 Result	14
3.4	Water inflow in a pellet box (test 3)	16
4	Model development for flow in pellet fillings	17
4.1	Earlier work	17
4.2	Piping model	19
4.3	Implementation	20
5	Modelling results and comparison to experimental experience	21
5.1	General behaviour compared to experimental experience	21
5.2	Modelling compared to the pellet box test	22
5.3	Modelling compared to 1 m deposition hole.	23
5.4	Summary of modelling of water flow in pellets	24
6	Mechanical model	25
6.1	Material model	25
	6.1.1 Fitting to Saturated conditions	26
	6.1.2 Fitting to un-saturated conditions	28
	6.1.3 Failure criteria	30
6.2	Swelling	31
6.3	Coupling between hydraulics and mechanics	32
7	Test of the mechanical model	33
7.1	Boundary conditions and geometry	33
	7.1.1 Geometry	33
	7.1.2 Hydraulic	34
	7.1.3 Mechanical	34
7.2	Results	35
	7.2.1 Swelling	35
	7.2.2 Influence of cracking	36
	7.2.3 Validity of the assumption of one way coupling	38
8	Conclusions	39
	References	41
Appendix 1	Comparison of modelled wetting pattern and measured, 0.1 l/min	43
Appendix 2	Comparison of modelled wetting pattern and measured, 0.01 l/min	45
Appendix 3	Derivation of boundary condition for the channel	47
Appendix 4	Data from uniaxial compression test on saturated samples of MX-80	49
Appendix 5	Data from uniaxial compression test on unsaturated samples of Bara-Kade 1002	53

1 Introduction

During the installation of buffer and backfill water will enter the deposition hole at different places and will be absorbed unevenly by the buffer. The inflows are mainly located in cracks in the deposition hole and the water enters in to the buffer as line or point sources. Often the system is simplified when saturation process is modelled with the total inflow spread out evenly over the entire deposition hole wall. There has been work done (Sandén et al. 2020) which shows that the swelling of the buffer not only depends on how big the inflow is but also on where the inflow points are located. The objective of this report is therefore to develop models that can predict how the buffer swells during the early stages after installation. Therefore both models that describe how water transports in pellet fillings and mechanical models are needed.

A key in understanding how the buffer will behave during the short time, which represent the installation time, is to be able to understand and predict the flow in the pellet filled slot between the buffer and the rock wall. Therefore development of mathematical models that describes the water flow in the pellet filling has been carried out. Most of the development work has been conducted within the EBS Task force framework. The development work done has earlier been reported in Eriksson (2019). In Eriksson (2019) the focus was mainly focused on development on models regarding vapour transport and advective water transport in the bentonite pellets. However, the transport of free water in the pore space between the pellets was also included.

The models developed earlier had the problem that the pellet filling sealed up after some time which resulted in that the water pressure increased towards infinity in the model which caused the model to break down. Therefore the model development in this report is focused on solving the problem of the pellets filling sealing up. This is done by adding channel formation to the model to describe piping in the material. A mechanical model is also developed to be able to describe the upwards movement of the buffer during the installation phase.

The installation phase in this report is considered to be approximately 90 days. In a real repository it is expected to take up to 50 days from the buffer is installed until the backfill is placed on top of the buffer depending on the installation sequence. But the first 90 days are evaluated to have some extra margins to the 50 days. Also the full scale tests done (Luterkort et al. 2017, Nord et al. 2020) to evaluate the effect of inflow on the buffer in the installation phase has been run for 90 days.

2 Water flow in pellet fillings

The process of inflow of water in bentonite pellet fillings seems to follow a quite complex pattern. The wetting pattern seems to be depending both on the inflow rate and on the properties of the pellets. The earlier modelling done in Eriksson (2019) a model that allows a flow of free water in-between the pellets was used. This model suggests that the following parameters would influence how the wetting pattern of the pellet filling will look:

- Suction of the pellets which can be correlated to the water content through the retention curve of the material.
- The geometry of the pellets.
- The air porosity in-between the pellets.
- The size of the pores between the pellets.
- Inflow rate of the water.

The suction of the bentonite pellet together with the permeability of the material will affect how quickly the water can be absorbed into the pellet. The absorbed water will make the pellet swell and start to seal the pores that exists between the pellets. Pellets with low initial water content have a larger suction and is expected to swell faster then a wet pellet initially. This is supported by Sandén and Jensen (2017) were it was observed that pellets with high water content absorbed water much slower which affected the wetting pattern.

The geometry of the pellets should in theory affect how fast water can be absorbed. A large pellet of a given shape should have a long transport path for the water to reach the centre of the pellet and therefore it should take longer timer to swell in to the pore space in-between the pellets. Also the amount of surface area compared to volume of the pellet should affect how quickly water is absorbed. Test were done in Lundgren and Johannesson (2020) where pillow shaped pellets with dimensions 15.8 mm × 15 mm × 7 mm were compared with extruded pellets with a diameter of 6 mm with similar water content. In these tests however, no differences between the two types off pellets could be seen.

It is likely that the flow resistance in the pellet filling depends on the porosity and the size of the pores. In packed beds without swelling pellets it has been shown that for example the Ergun equation can approximate the flow resistance rather well. This equation is based on Reynolds number and can describe both the laminar and turbulent flow regime. This equation is also used in the models in this report to predict the flow resistance. The flow resistance model is calibrated against measurements made in Luterkort et al. (2017) where flow resistance was measured for air flows as a function of flow velocity and density of the pellet filling. This model suggests that a decrease in porosity should increase the flow resistance. In the same way as the size of the pores decrease the flow resistance increases, even if the air porosity is kept constant. This is supported by tests done in Andersson and Sandén (2012) where granules with similar density as pellets were tested and the tests showed that the granules sealed much faster.

The influence of inflow rate has been studied in several reports, for example Åberg (2009) and Sandén and Börgesson (2010). A summery of how different inflows behave in a pellet filling was done in Börgesson et al. (2015) where different observed inflow pattern was correlated to certain inflow rate regimes. The transition between the different inflow regimes are assumed to be smooth although the exact limit were the behaviour changes is not known. The observed behaviour was described with the following inflow rate regimes:

$q \geq 0.1 \text{ L/min}$

At very high inflow rates, the water inflow is faster than what the individual pellets can absorb so the free water will fill up the empty pore space and by gravity flow downwards. The deposition hole will be filled like a bathtub.

$q = 0.01 \text{ L/min}$

At fairly high inflow rates, the flow is spread equally in all directions and thus fills the slot circularly with the inflow point as centre and with increasing radius with time. There might though be a tendency for upwards movements. When the water reaches a free surface it seems as the continuing flow mainly goes to the surface.

$$q = 1.0 \times 10^{-3} \text{ L/min}$$

At low inflow rates, the flow seems to move upwards in a rather narrow channel. Once it reaches a free surface of the pellet filling, the water stays there and continues to flow out on the surface. The reason for the upward flow is not clear.

$$q = 1.0 \times 10^{-4} \text{ L/min}$$

At very low inflow rates, the inflow pattern seems to go back to something between the pattern at 1.0×10^{-3} L/min and 0.01 L/min. An elliptic pattern seems to be formed with a tendency to move upwards and the major axis directed vertically.

$$q \leq 1.0 \times 10^{-5} \text{ L/min}$$

At extremely low inflow rates, the water seems to follow a diffusion-like behaviour and spread as concentric circles, similar to that at 0.01 L/min.

The conceptual model developed in Börjesson et al. (2015) is illustrated in Figure 2-1.

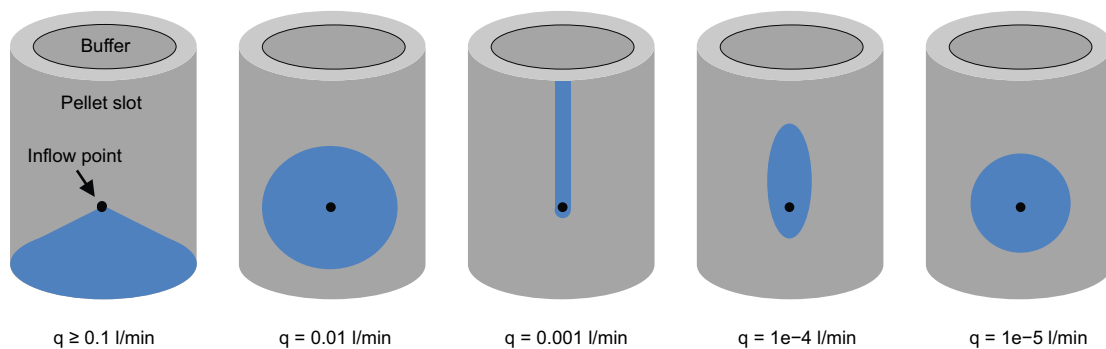


Figure 2-1. Illustration summarizing the knowledge of how inflow rate effects the wetting pattern form (Börjesson et al. 2015).

3 Earlier tests

3.1 Test used to compare the model with

As mentioned earlier a number of experimental studies have been done earlier. This report has focused on the result from a few of them to use as cases to test the numerical models for water inflow in pellet fillings. The first one (test 1) is a test reported in Åberg (2009) in which the effect of water inflow on two full scale blocks surrounded by a pellet filled slot were tested. The result from this test is summarized in Chapter 3.2. This test was suitable because data was recorded both on the wetting pattern of the pellet filling but also on the upwards displacement of the buffer blocks. It should therefore be possible to see how well an inflow model would work together with a mechanical model to predict the upwards movement of the block.

The second test (test 2) chosen is a similar test as the first one. The major difference is that a weight of 10 tonnes was added on top of the setup to simulate buffer blocks further down in the deposition hole. Also a smaller inflow was used in one of the setups. This test has not been reported earlier but a short description of the test and the results are shown in Chapter 3.3.

The final test (test 3) that is used to test the models in this report is a pure pellet inflow test where wetting patterns were recorded for different inflows, pellet type and two different materials. The data used in this report is described in Chapter 3.4 and the details of the test can be found in Lundgren and Johannesson (2020).

The first two tests, test 1 and test 2 were chosen because they are in full scale and that the wetting pattern was recorded in a way that it is easy to compare with modelling results and because the swelling of the buffer blocks were measured. These are serving as good examples to test both the models for water transport in pellet fillings and the mechanical model. Test 3 is used because it has a simple geometry with relatively clear boundary conditions. This makes it easy to compare and use to develop the model for water transport in pellet fillings.

3.2 Water inflow in a 1 m section of a deposition hole (test 1)

This test is reported in detail in Åberg (2009). The test setup consists of a 1 m high container of acrylic glass with the same diameter as a full scale deposition hole, 1 750 mm. Inside the container two 500 mm high buffer rings were placed which had a diameter of 1 650 mm. The surrounding slot between the container and the buffer blocks was filled with pellets. Therefore the test would represent a 1 m part of a full-scale deposition hole. A point inflow was located at mid height of the container on one side. The test was thereafter run with two different inflows, 0.1 l/min and 0.01 l/min. During the test the wetting pattern and the deformations of the top block was recorded. The wetting pattern for 0.1 l/min is shown in Figure 3-1 and for 0.01 l/min in Figure 3-2. The displacement of the upper surface of the top block is shown in Figure 3-3.

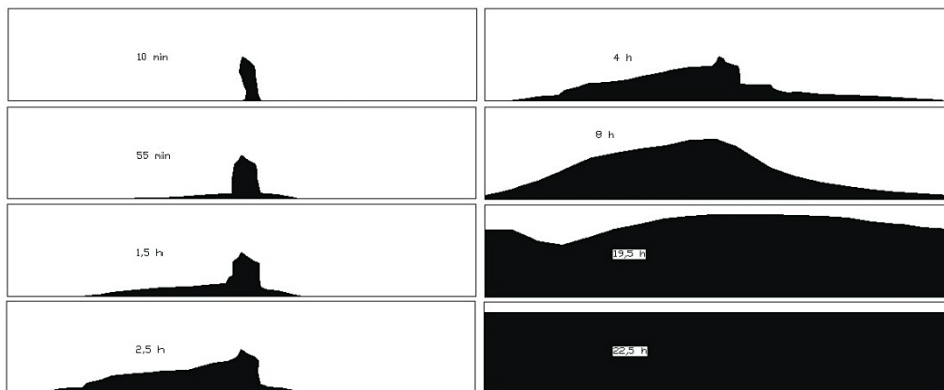


Figure 3-1. Inflow pattern from an inflow of 0.1 l/min taken from Åberg (2009).

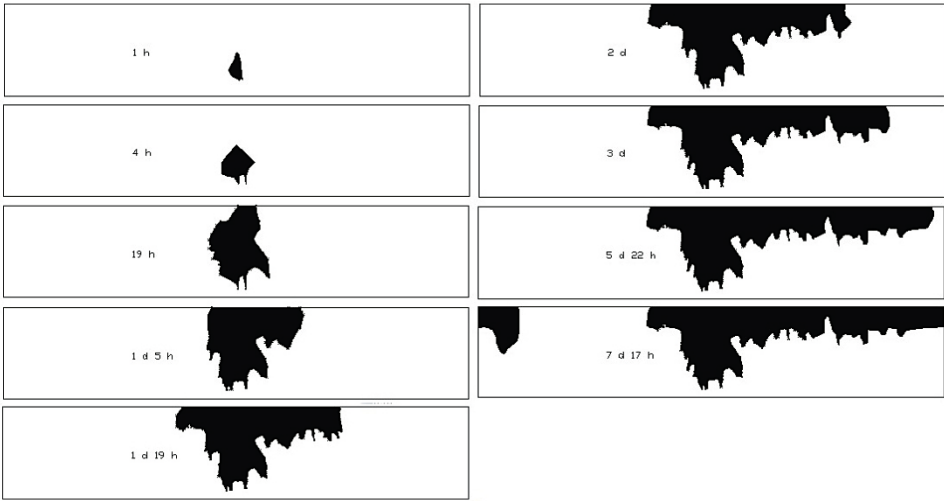


Figure 3-2. Inflow pattern from a inflow of 0.01 l/min taken from Åberg (2009).

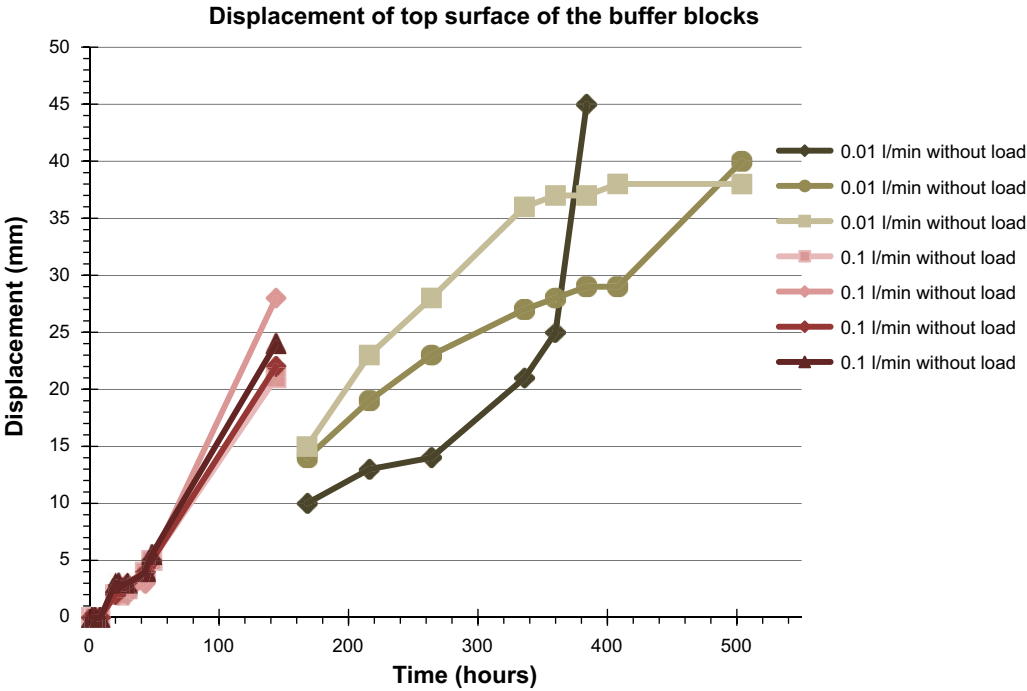


Figure 3-3. Displacements of the top block in the two tests.

3.3 Water inflow in a 1 m section of a deposition hole with extra weight (test 2)

3.3.1 About the test

After the test described in Chapter 3.2 some more test were done. The same setup was used but a weight of 10 tonnes was placed on top of the upper block, se Figure 3-4. Also a system of displacement sensors was used instead of manual measurement of the top surface displacements. The 10 tonnes was meant to simulate five buffer blocks lying above the test section. This means that the test should be representative for two blocks positioned at the top of the canister.

3.3.2 Setup

The test container and water inlet equipment was identical to the setup used in Chapter 3.2 and more information is found in Åberg (2009). The test was done with two different inflow rates, 0.1 l/min and 0.001 l/min. The big difference with this test was the influence of weight on top of the block which would simulate a block further down in the buffer. The test setup is shown in Figure 3-4. The displacement of the top surface was measured with displacement sensors at three locations with an angle of 120° in-between. To allow the sensor to have enough room the sensors were placed on arms outside the block. This placement will make any tilting of the block exaggerated. But since the positions are known and the top plate acts like a plane the positions can be recalculated the block edges.

The main focus was to look at the displacement of the top surface of the block and therefore the wetting pattern was not mapped but photographs were taken which gives an indication how the wetting looked like.



Figure 3-4. Picture showing the setup. Two buffer blocks with pellet filled slot around with 10 ton of weight on top. The hoses in the top of the container are drainage pipes and the inflow point is seen to the left.

3.3.3 Result

The displacement for the top block is shown in Figure 3-5 for both inflows. Since there was a malfunction on one of the displacement sensors (at 0 degrees) there is a gap in the data where no relevant result can be displayed. This is because two measurement points is not enough to recalculate the displacement of the block. In the figure the displacement data from the test described in Chapter 3.2 is also displayed as comparison. The result shows the displacement is reduced when a weight is placed on top of the blocks. The test with an inflow of 0.1 l/min had a very similar wetting pattern as the test in Chapter 3.2. For 0.001 l/min the wetting seems to be mainly around a vertical line from the inflow point and thereafter distributed out over the top surface, see Figure 3-6. However, the water seems to flow in the direction towards the measurement at 240 degrees. This is why the displacement at 120 degrees is lower than the others and the pellet fulling at that position is almost dry, see Figure 3-7.

After the test time the setup were disassembled and cracks were documented. The upper block had cracks through the whole block while the lower block had very little cracks through the block. There were also a lot of cracks in the corners at the outer diameter of the upper block, see Figure 3-8.

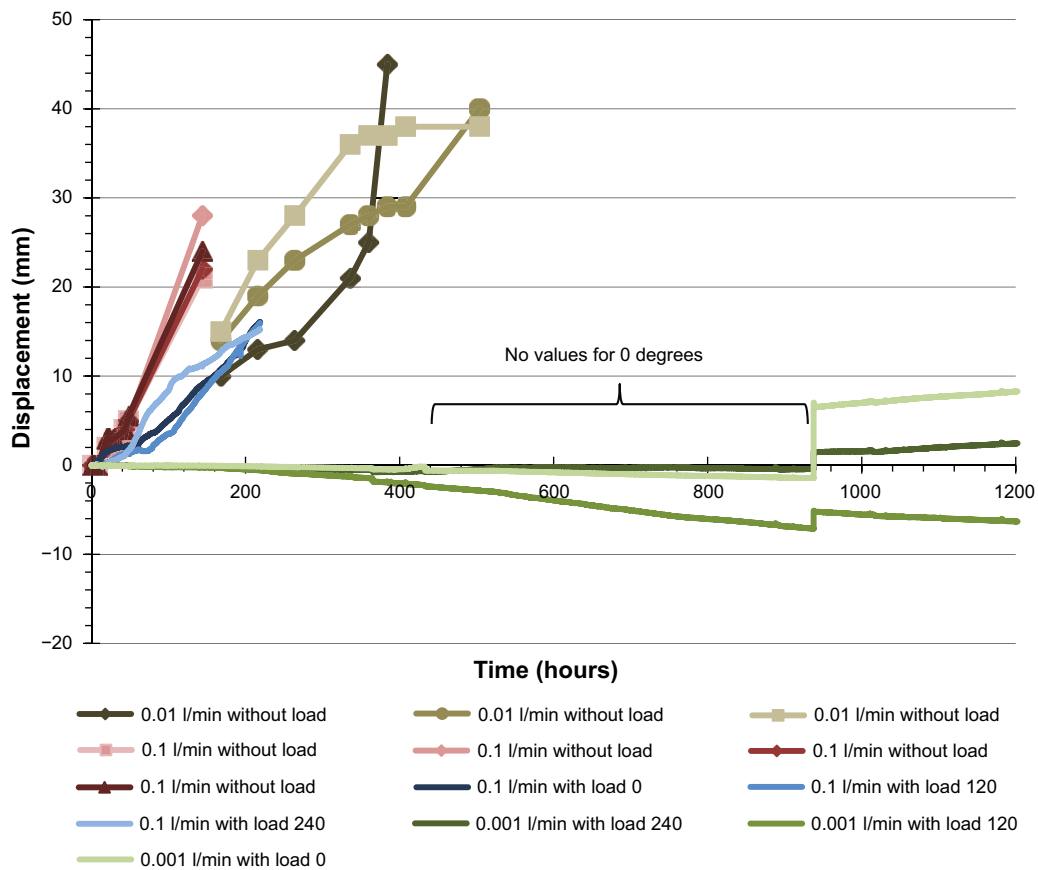


Figure 3-5. Measured displacements of the top block. The result from the test Chapter 3.2 is also added for comparison. Note that the values for the measurements with load are recalculated to represent the movement at the block edge, that is why when one sensor failed all the results are wrong.



Figure 3-6. Picture The wetting pattern for an inflow of 0.001 l/min. the water initially goes upwards until it reaches the top surface and the water starts to spread over the top surface. The picture is taken approximately 40 days after the test was started.



Figure 3-7. Picture showing the dry pellets around 120 degrees.



Figure 3-8. Picture The wetting pattern for an inflow of 0.001 l/min. the water initially goes upwards until it reaches the top surface and the water starts to spread over the top surface. The picture is taken approximately 40 days after the test was started.

3.4 Water inflow in a pellet box (test 3)

This test is basically done in a box which has a pellet slot with the dimensions $1 \times 1 \times 0.05$ m. The thickness of the test is the same as the expected for the pellet slot in a real deposition hole. The details about the test are reported in Lundgren and Johannesson (2020). In the pellet box different inflow, pellet type and material was tested. This report focus on the results with roller compacted pellets made from Bara-Kade 1002 which is a Wyoming clay similar to MX-80 which has been use earlier and therefore most of the material data is available. The inflow has been varied between 0.1 l/min to 0.001 l/min. These tests have earlier been used to test the models developed to predict wetting pattern form different water inflows (Eriksson 2019). In this report the focus is on the tests done with roller compacted pellets of Bara-Kade 1002. The result from these tests gives mostly the same result as earlier tests. The results from 3 different inflows are shown in Figure 3-9.



Figure 3-9. Wetting patterns for three different inflows 0.001 l/min, 0.01 l/min and 0.1 l/min. The lowest inflow to the left and the highest inflow to the right.

4 Model development for flow in pellet fillings

4.1 Earlier work

A model had already started to be developed (Eriksson 2019) and in that model flow of water is allowed in the pore space in-between the pellets. This is calculated as a two phase Darcy flow which model the free water in the pore space and with Richards equation which describes water transport in the clay. The two-phase Darcy equation is coupled to the Richard equation by allowing water to be transported from free water to the clay but not the other way. The absorbed water is also used to calculate the air filled porosity which affects the flow resistance in the two-phase Darcy equation. The flow resistance is calculated with Ergun equation found in Eriksson (2019) which can be recalculated to permeability and used in the two-phase Darcy equation. However, since Darcy flow can only have permeability which is independent of velocity only the linear term of the Ergun equation is used. In this model the absorption rate is assumed to be proportional to the difference suction between free water, in this case zero and the average suction of each pellet which is the suction calculated in the Richard equation.

This model gave rather good results for high inflow of 0.1 l/min and also for the first couple of hours for 0.01 l/min, see Figure 4-1, but the after a certain time the air filled porosity goes towards zero and this causes the flow resistance to go towards infinity and therefore also the water pressure goes toward infinity, see Figure 4-2. This causes numerical errors and continued calculation of the model is not possible.

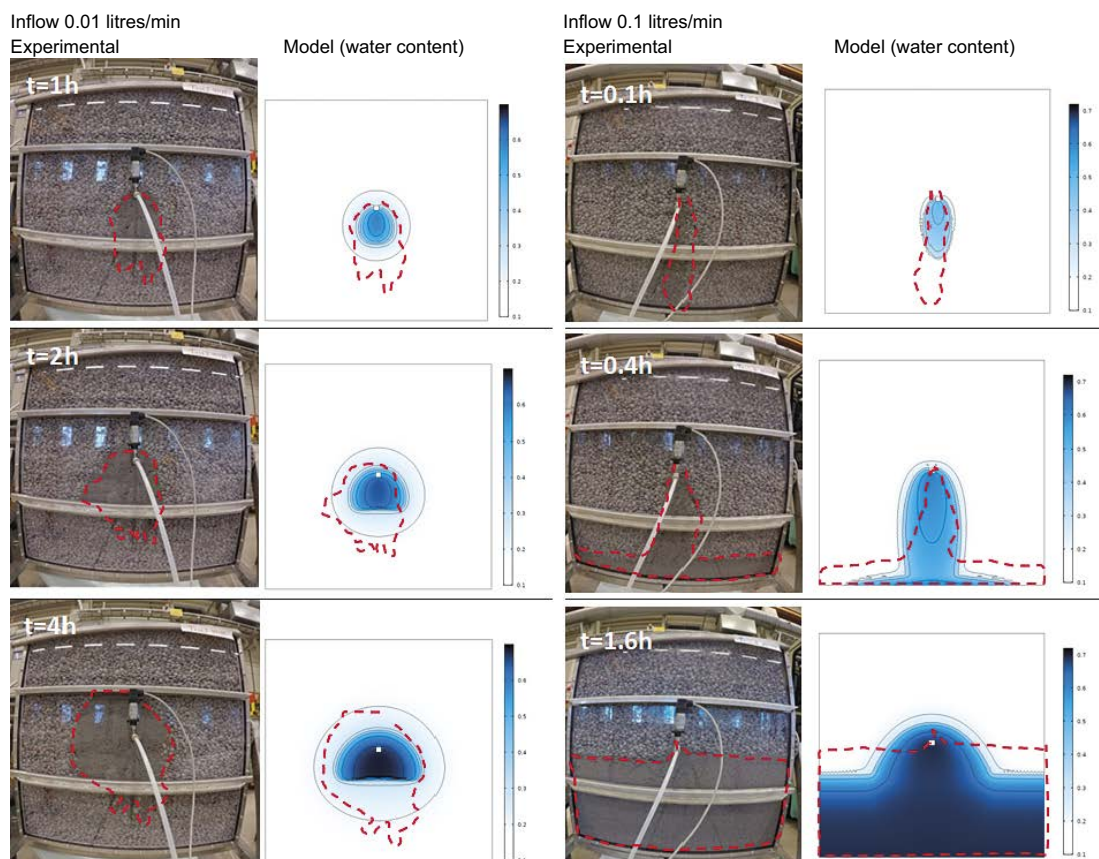


Figure 4-1. Modelled inflow patterns for the model without a piping model compared to tests.

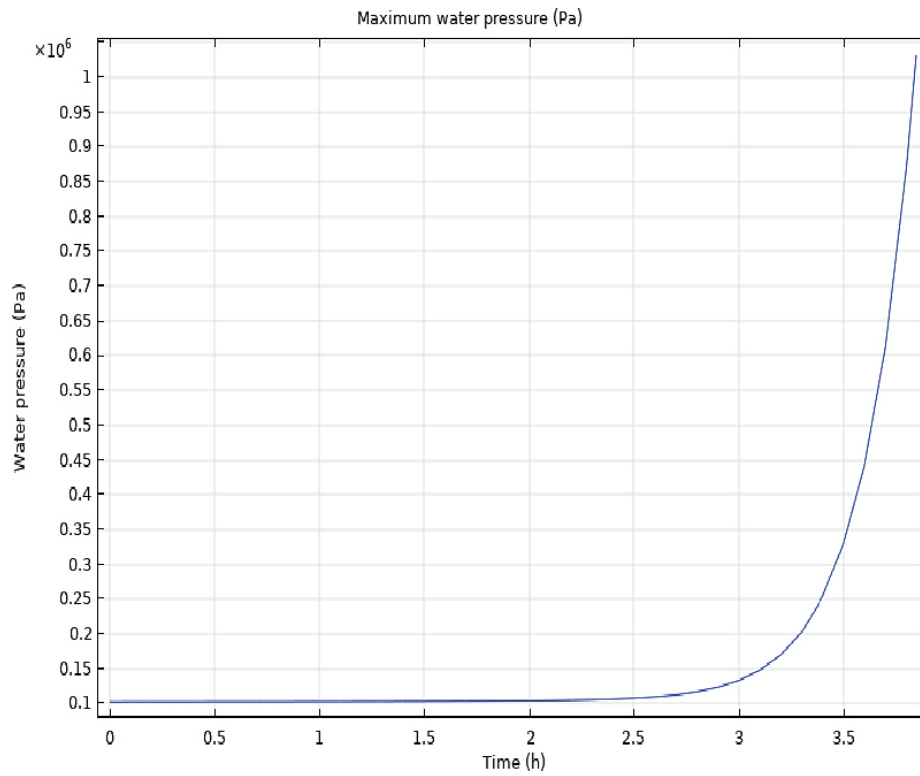


Figure 4-2. Pressure evolution for an inflow of 0.01 l/min without a piping model.

As the pellets seal in a real system the pressure will increase up to a certain point and then a channel is formed and the pressure is released. This phenomenon is called piping. To be able to handle pressure increases due to sealing of the pellets a piping model needs to be added.

4.2 Piping model

In this chapter the piping model used are described. The strategy to model piping is to allow water pressure to increase up to a certain level and when this pressure is reached a channel segment will be formed. The basic steps for the calculation are shown in the process flow diagram in Figure 4-3. The simulation is running as usual until maximum water pressure condition is fulfilled, which is set manually before the simulation starts. When this happen the simulation stops and the geometry is updated with a channel segment. This is done by evaluating the last time step finding the direction of the maximum flow velocity at the end of the channel. A segment of a channel is then added, in the same direction as the maximum flow velocity, to the existing pipe or to the inflow point if it is the first channel segment. The length of the channel segment has in this model been taken to be constant to 5 cm. This can be done in a more elaborate way by evaluation the pressure gradient around the channel. But to keep the model simple and avoid to many updates in the geometry the constant length approach has been used. Finally the boundary conditions are updated before the simulation is restarted with the new geometry and an initial condition. The new initial condition is the same as the condition before the geometry was updated.

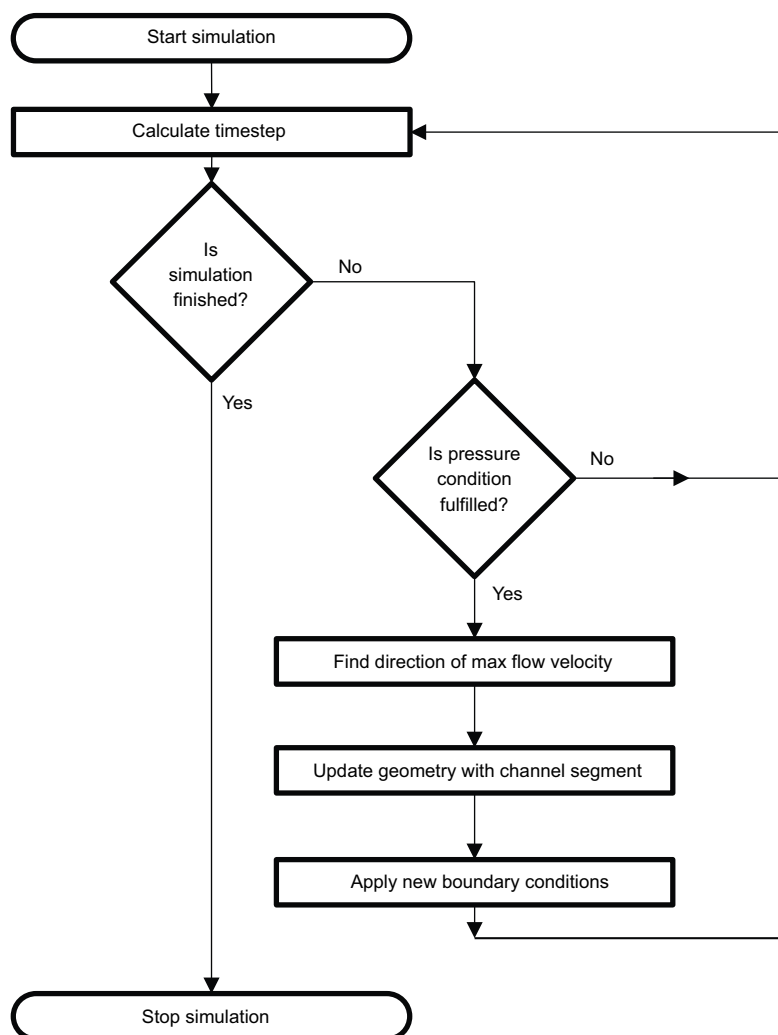


Figure 4-3. flow diagram used in the simulation.

There is also a need to describe the boundary condition of the channel to make it behave similar to a real channel. The channel needs to let water pass the walls of the channel along the whole length. However the largest flow should be where the air filled porosity is largest because there the flow resistance is the lowest. To calculate the water flow from each position along the pipe an analogy to ohms law is used. According to Darcy law the flow rate can be described by Equation 4-1. From this it could be identified that Q would be equal to the current, μ/κ is the resistance and $-dp/dx$ is the voltage.

$$Q = -\frac{\kappa dp}{\mu dx} \quad \text{Equation 4-1}$$

If the pressure gradient is assumed to be constant along the channel then a flow rate can be calculated by approximating the channel as an infinite amount of resistors mounted in parallel. Then the Equation 4-2 can be used to describe the flow perpendicular to the channel as a function of its distance from the starting position. A detailed derivation of Equation 4-2 can be found in Appendix 3.

$$\frac{\kappa(l)}{\int_0^l \kappa(l) dl} \frac{q_{inflow}}{t} \quad \text{Equation 4-2}$$

Where t is the thickness of the pellet slot, if a 2D model is used, κ is the permeability, L is the total length of the pipe and l is the lengths coordinate along the channel.

4.3 Implementation

The model is implemented in COMSOL Multiphysics. To be able to use the process described in Figure 4-3, a function called “Model Methods” in COMSOL is used. A JAVA program is written which calls the COMSOL API to update the geometry and boundary conditions of the model. As mentioned earlier a specified pressure is used as a criterion for the channel formation, in this case 15 kPa. 15 kPa was chosen as a criterion for channel formation to match experimental results, see Figure 5-3. The length of each channel segment is fixed to 5 cm. if the channel exits a boundary then the model is either stopped or the model is adjusted to allow for water to flow on the top surface of the pellet filling. The criterion for channel formation could be change to a pressure gradient instead. Also the channel segment length could be changed or be physics dependent but for the modelling done in this report criterion for maximum pressure and a fixed channel segment length is used for simplicity.

5 Modelling results and comparison to experimental experience

5.1 General behaviour compared to experimental experience

Due to the implementation of a piping model the model can now be run for long times with a wide range of inflows. The model has been tested with point inflows from 0.1 l/min to 1×10^{-5} l/min and they all seem to predict reasonable wetting of the bentonite pellet filling. The result is shown in Figure 5-1 where it is compared with the conceptual model from Børgesson et al. (2015).

The black line in the model figures represents the formed channel. One would expect it to be straight up but there are some mesh dependence due to that the flow is so small and it is difficult to use a mesh fine enough to totally remove this. However, this can be used to model the randomness of the properties of the pellet fillings. One interesting observation is that all channels that are formed seem to grow upwards. In the model this is explained by looking at the flow at the end of the channel. As water first enters the system it starts to flow downwards due to gravity. As the pellets below the inflow starts to seal the flow instead start flowing to the sides and finally as this part also starts to seal the flow starts to go upwards. The final step is when even the part above the inflow starts to seal and the pressure start to increase. At a defined pressure a channel start to form and since the pellets above the inflow has had the shortest time to seal the flow resistance lowest in that direction. The water tends to follow the path of least resistance and therefore the channels tend to grow upwards.

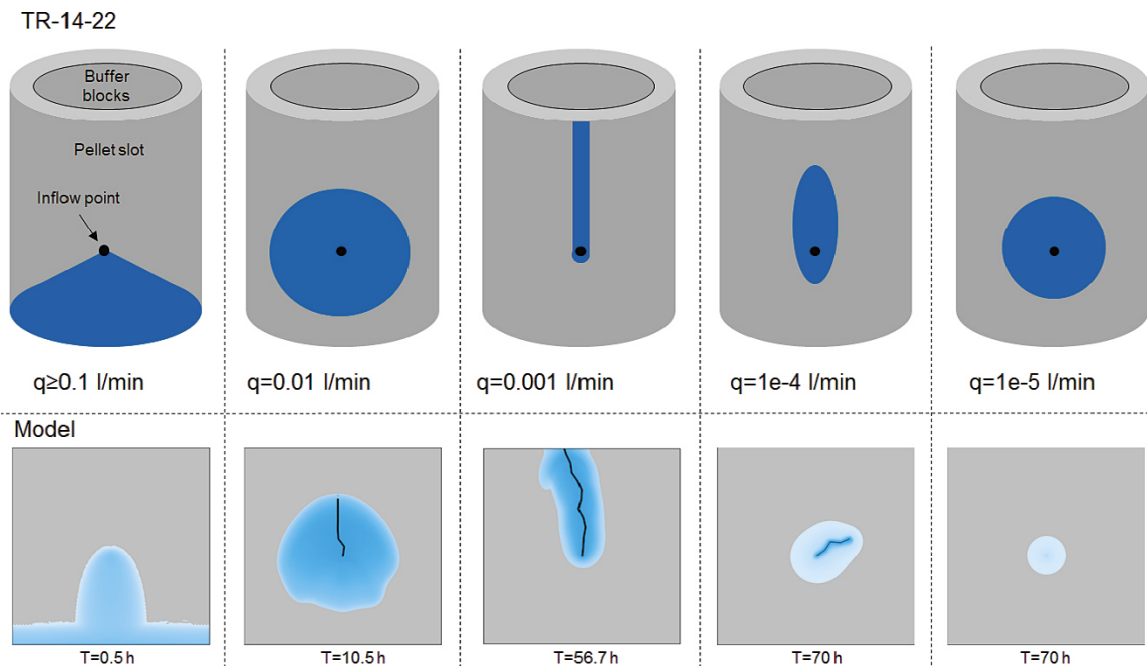


Figure 5-1. Model with included piping model (bottom row) compared to the conceptual model in Børgesson et al. (2015), top row.

5.2 Modelling compared to the pellet box test

The wetting pattern has documented at several different times during the test which makes it possible to compare the time evolution of the test. The model has been compared with the test at an inflow of 0.001 l/min in Figure 5-2. It looks like a channel has formed in the test which goes out to the left in the beginning (between 10 h and 20 h). Later it looks like that channel has sealed of and a new channel have formed. The model is stopped after 57 hours due to that the pipe has reached the top surface. In the test however the water reaches the top after 72 hours. There is a difference in 15 hours for the water to reach the top surface between the model and the test. This is likely due to that the water goes out to the left in the beginning of the test which it does not do in the model.

For 0.1 L/min the model has already been compared with the test since at this flow the whole container fills up quickly and the pellets have very little time to swell and therefore the result should be the same as the model without piping model, Figure 4-1.

The inflow water pressure was also measured during the test. The model and the test pressure evolution are compared in Figure 5-3. The model has a more on-off behaviour but it is likely that this would be more realistic if shorter channel segments were used but that would also increase the computational cost. It should also be noted that in the model the channel itself has no flow resistance, in real life there should be a flow resistance which would increase with the length of the channel.

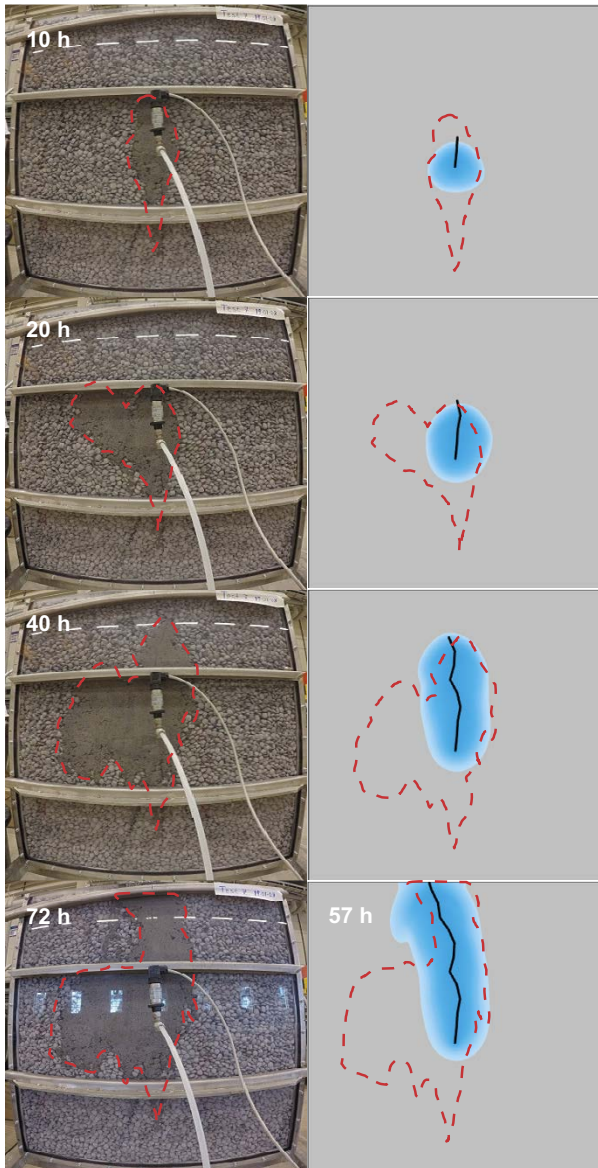


Figure 5-2. The modelled result compared to experiment with an inflow rate of 0.001 l/min.

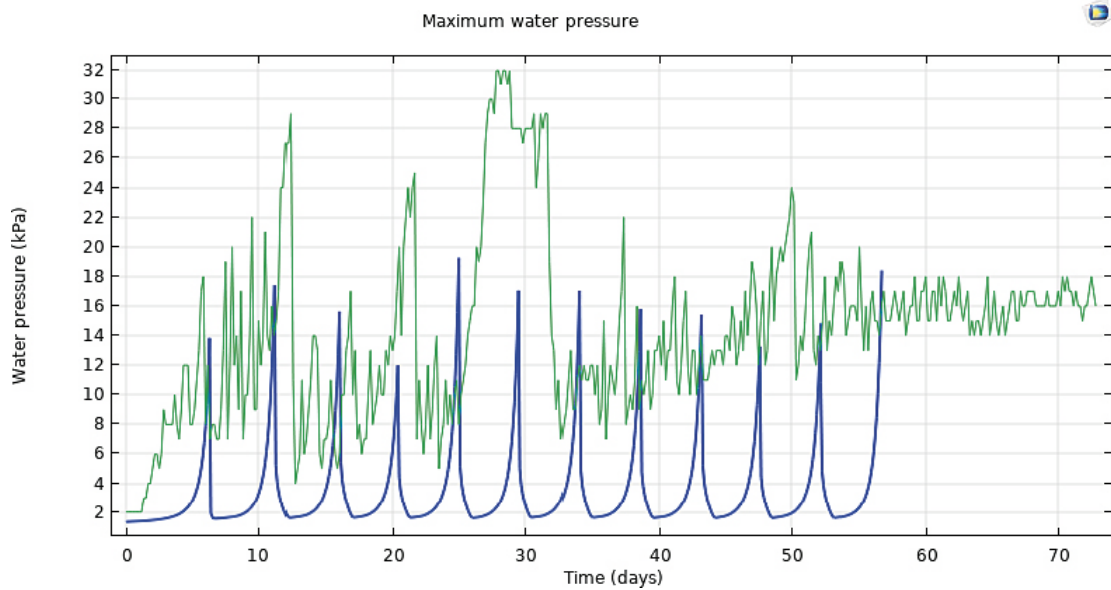


Figure 5-3. The modelled water pressure (blue line) compared to experiment with an inflow rate of 0.001 l/min (green line).

5.3 Modelling compared to 1 m deposition hole.

When modelling the tests from Chapter 3.2 some extra assumptions need to be added to the model because after a while the water reaches the surface and starts to flow out over the surface. To try and model this, a domain is added on top of the pellet filled slot. This domain is modelled as a porous media with high hydraulic conductivity (10^{-7} m/s) and as a non swelling material, see Figure 5-4. So when the water reaches the top it will start to distribute over the top surface. However, in the real test there is drainage and also it is not known how even the top surface of the pellet filling looks like. So the model will most likely overestimate the amount of water coming from the top surface.

Since the slot is cylindrical and connected in the right and left boundary, a boundary condition is used that maps the outflow on one boundary and sets it as an inflow on the other. The model result is compared with the data from the test for the inflows 0.1 l/min and 0.01 l/min in Figure 5-5 and Figure 5-6 for a few different times. For comparisons at more times see Appendix 1 and Appendix 2. The model works satisfying although there are some uncertainties in the test setup which makes it difficult to set realistic boundary conditions.

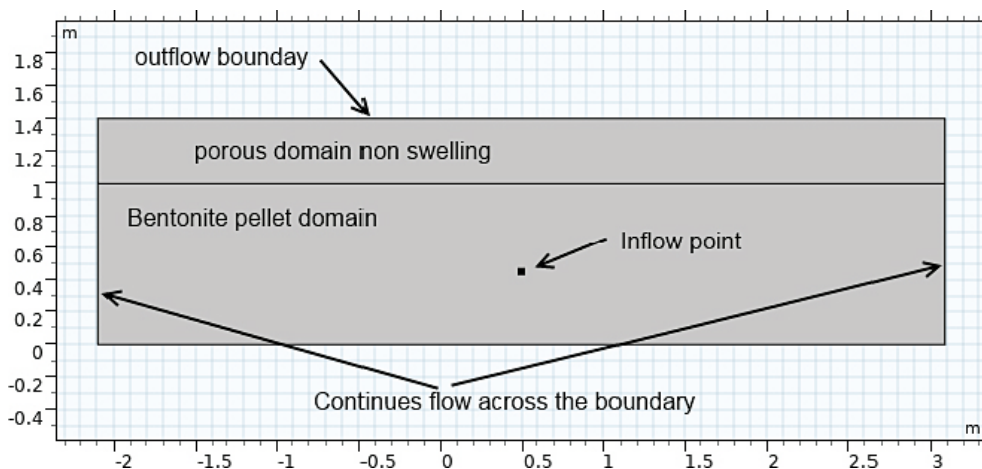


Figure 5-4. Model setup used to capture the flow of material on the top surface. An outflow boundary is place in the top to let air out.

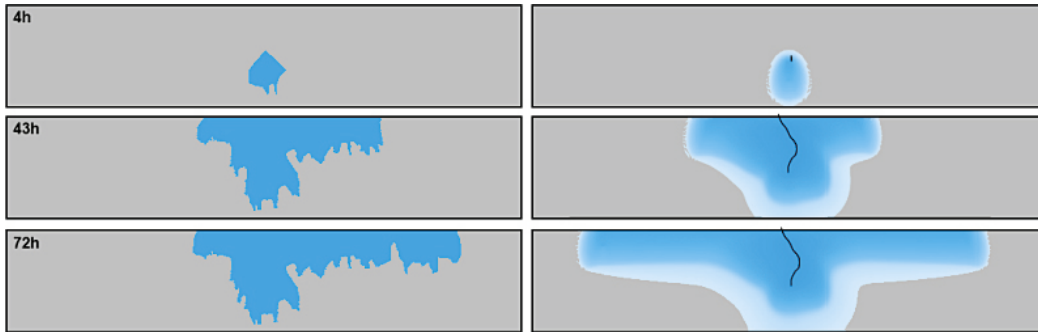


Figure 5-5. Modelling result, right side, compared to test, left side, at a water inflow of 0.01 l/min for three different times.

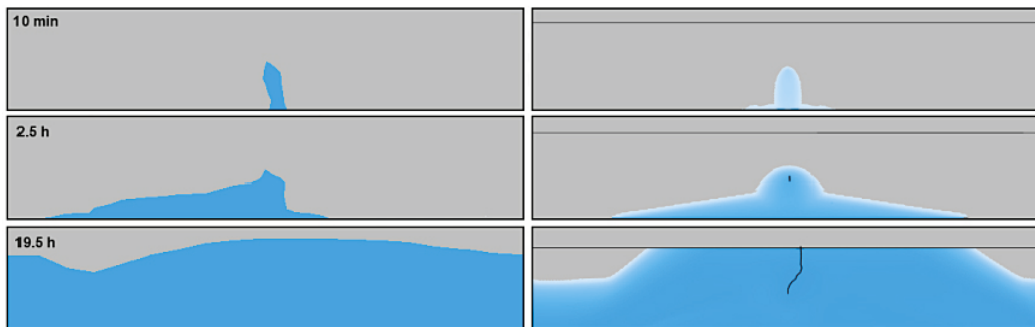


Figure 5-6. Modelling result, right side, compared to test, left side, at a water inflow of 0.1 l/min for three different times.

5.4 Summary of modelling of water flow in pellets

The result from the modelling gives rather good agreement with experimental result. The model also explains the different behaviour in different inflow rate. However, there are some randomness to the distribution of pore sizes and dry density of the pellet filling which has to be considered when comparing the model with experiments. A random field for these properties could be added to get a more realistic behaviour but it is currently not known how a realistic distribution looks like. It is believed that the model captures average behaviour of the pellet filling well and gives a possible explanation for why the wetting pattern looks different for different inflows.

6 Mechanical model

6.1 Material model

To be able to predict the movements of the buffer during the installation phase depending on which inflow the deposition hole has, a mechanical model has been developed. The model can then be connected with the pellet flow model in Chapter 5 to try and predict the swelling of the buffer during the installation phase when inflows to the deposition hole are in form of line and point sources. A non-linear mechanical model is derived from uniaxial compression tests done. Two datasets has been used to develop and calibrate the model. One dataset which is done on saturated samples of MX-80 which is published in Svensson et al. (2019) and also shown in Appendix 4 and one dataset which has been performed on unsaturated samples of Bara-Kade 1002 which is shown in Appendix 5.

The material model chosen for this case is Ramberg-Osgood which has a stress-strain relation that is shown in Equation 6-1.

$$\varepsilon = \frac{\sigma}{E} + \alpha \frac{\sigma}{E} \left(\frac{\sigma}{\sigma_0} \right)^n \quad \text{Equation 6-1}$$

The parameters σ_0 , α , E and n can all be considered to be a function of water content and air-filled porosity: $\sigma_0(w, \varphi_a)$, $\alpha(w, \varphi_a)$, $E(w, \varphi_a)$ and $n(w, \varphi_a)$. Where w is water content (mass of water divided with dry mass) and φ_a is air-filled porosity. To find out what these functions are a computer program was written that evaluates these parameters with a multivariable regression for each individual stress-strain curve from the uniaxial compression tests. In order to get a better fit the initial part of the curve and the softening region were removed because this is not captured by the model. When the parameters have been found for each curve a suitable function is used to approximate the values. Since the range in water content and air-filled porosity is limited in the data used the values out side the maximum and minimum values are uncertain. It should also be noted that α and σ_0 are not independent of each other so α could be changed if σ_0 is changed as well. Therefore α is considered constant at the value 0.02.

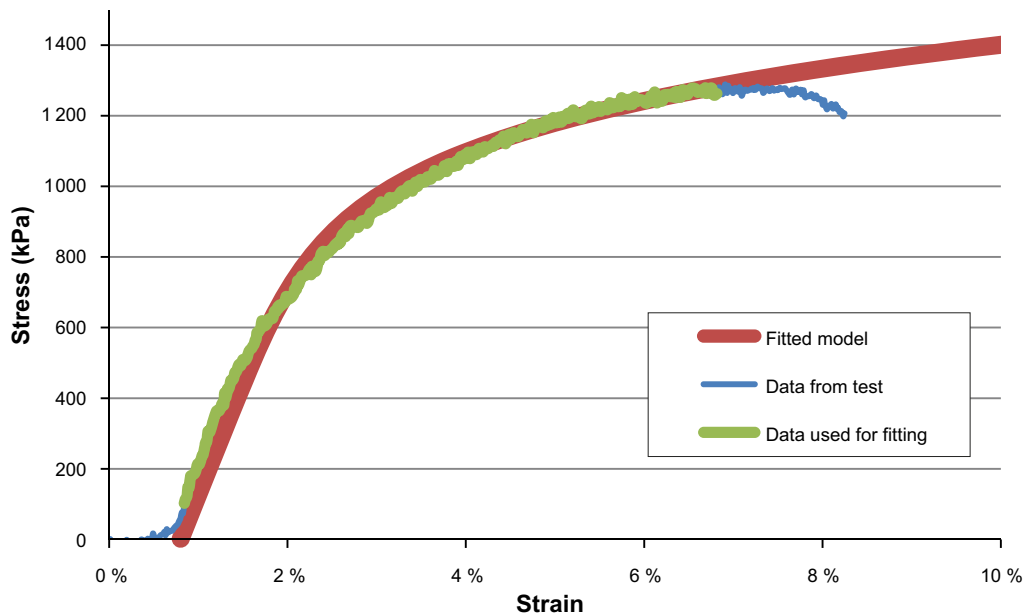


Figure 6-1. Data from uniaxial compression test (blue line), the data range used for fitting to Equation 6-1 (green line) and Equation 6-1 fitted to data (red line). This is for a saturated sample with water content of 32.7 %.

6.1.1 Fitting to Saturated conditions

An example of a fitting of Equation 6-1 to the data is shown in Figure 6-2, in this case a saturated sample with water content of 32.7 % was used. In the figure three curves can be seen, one is the original stress-strain curve from the test, one is the stress-strain from the test representing the data used for fitting and finally the fitted function. The data for all tests used are shown in Appendix 4.

The parameters E , σ_0 , and n are plotted in Figure 6-2 to Figure 6-4 together with a suggested function to describe these parameters as a function of water content. For the yield stress some data has been recalculated from compaction tests according to Equation 6-2, which is taken from Eriksson (2017). In Equation 6-2 σ_f is the flow stress, φ_a the air filled porosity and p is the compaction pressure. This calculation assumes that the material is a perfectly plastic material. The samples are unsaturated, however, the model only considers the material around the pores and this can be considered saturated.

$$\sigma_f = \frac{3}{2} p \frac{\varphi_a}{(1-\varphi_a)} \quad \text{Equation 6-2}$$

If these functions are used in Equation 6-1 then the model is shown in Figure 6-5 together with the measured values.

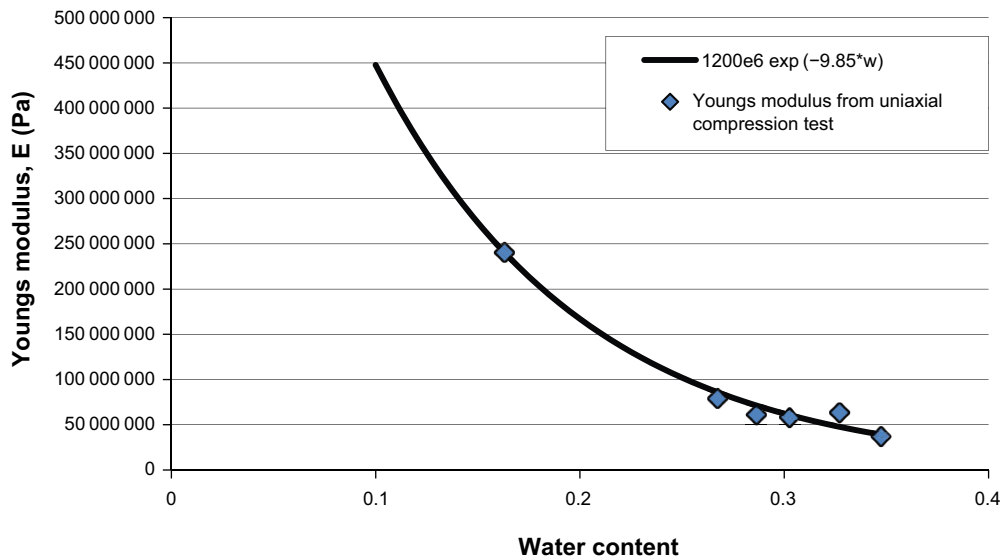


Figure 6-2. Young's modulus from fitted data for different water content and a suggested function of water content to describe this.

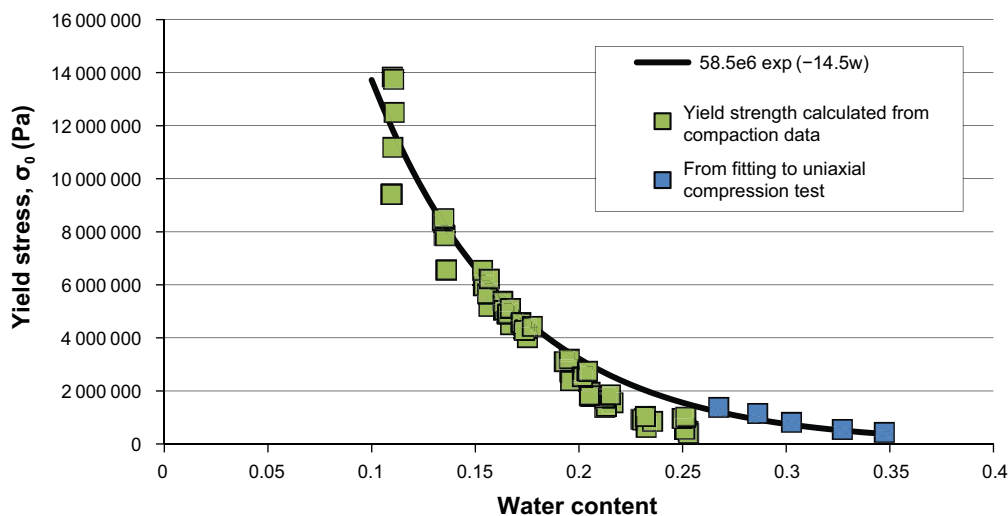


Figure 6-3. Yield stress from fitted data for different water content and a suggested function of water content to describe this.

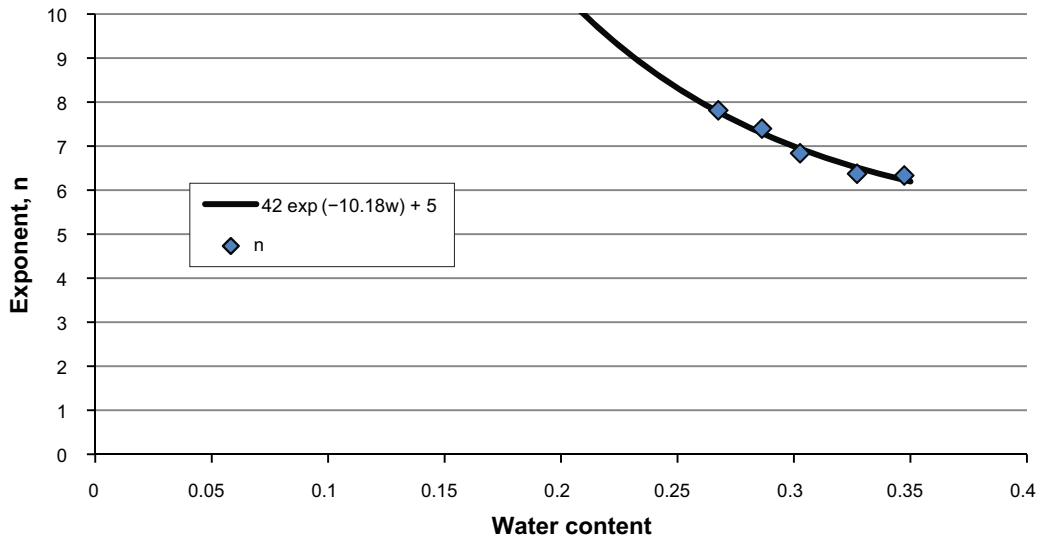


Figure 6-4. n from fitted data for different water content and a suggested function of water content to describe this.

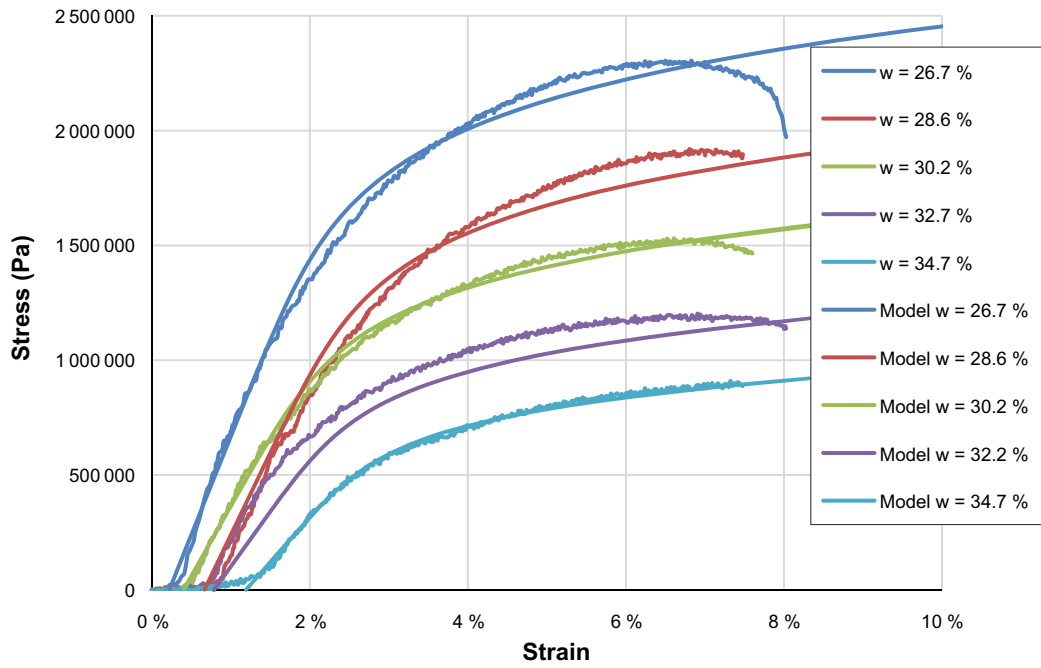


Figure 6-5. The combined model compared to data (Appendix 4).

6.1.2 Fitting to un-saturated conditions

The same method was used as in the saturated case to fit against air-filled porosity. Often an exponential expression with porosity is used to describe strength of porous materials. Therefore this is used in this model as well. At zero air-filled porosity the model should go back and give the same values as the saturated case. The parameters for different air-filled porosities is plotted in Figure 6-6 to Figure 6-8 together with the suggested fitting function. The total model is plotted against the experimental values in Figure 6-9. In the limited dataset used here it seems that α and n is independent of the air-filled porosity.

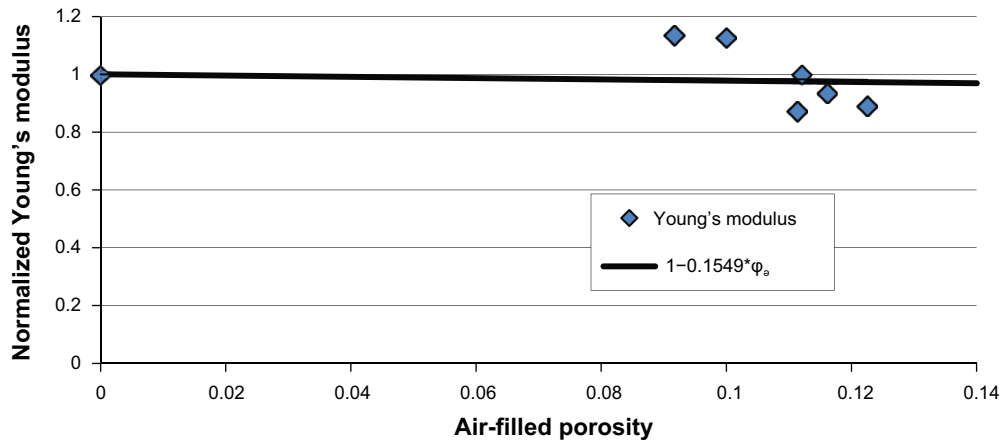


Figure 6-6. Young's modulus from fitted data for different water content and a suggested function of air filled porosity to describe this. The Young's modulus is normalized with the Young's modulus for the saturated case.

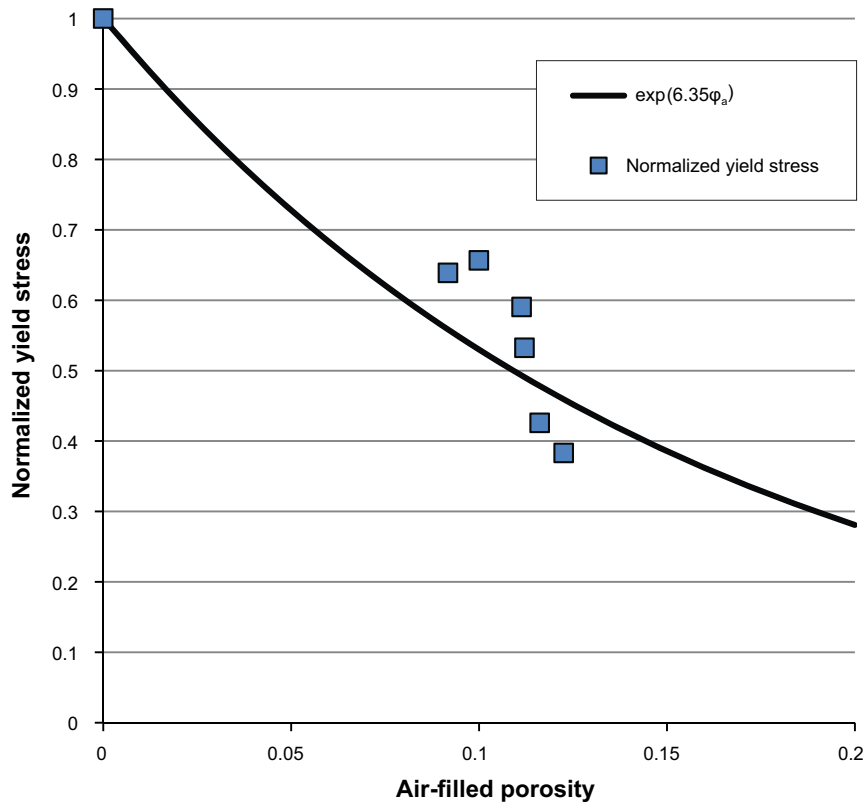


Figure 6-7. Yield stress from fitted data for different water content and a suggested function of air filled porosity to describe this. The yield stress modulus is normalized with the yield stress for the saturated case.

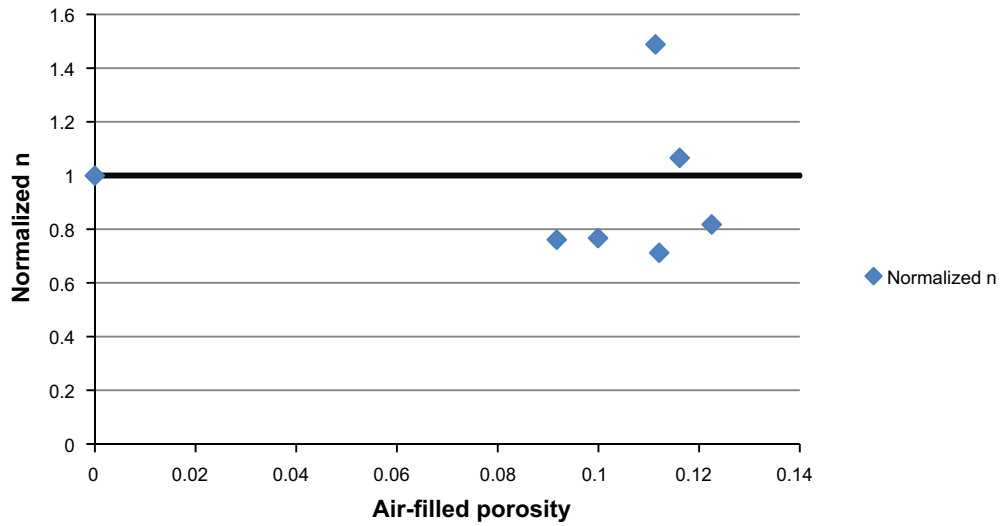


Figure 6-8. n from fitted data for different water content and a suggested function of air filled porosity to describe this. The n is normalized with n for the saturated case.

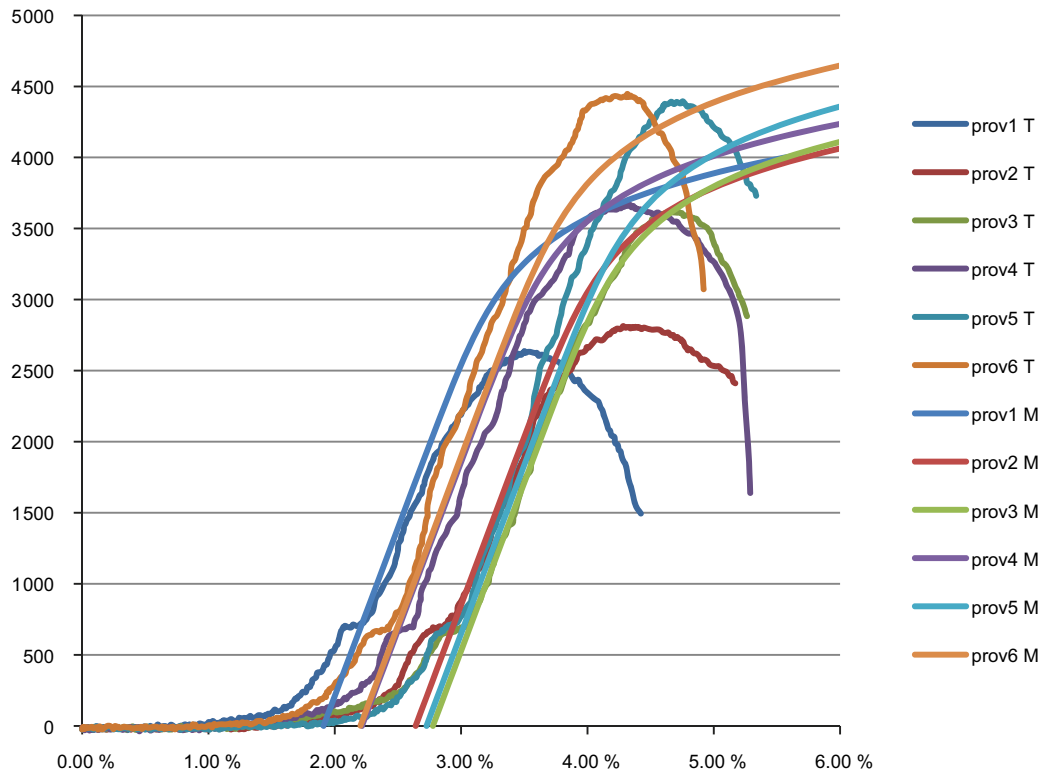


Figure 6-9. The model for the unsaturated case compared to the uniaxial compression test. (Appendix 5).

The total model can now be described with Equation 6-1 with the following functions for σ_0 , α , E and n.

$$\sigma_0 = 58.5e6 \exp(-14.5w) \exp(-6.35\phi_a) \quad \text{Equation 6-3}$$

$$E = 1200e6 \exp(-7.85w)(1 - 0.1549\phi_a) \quad \text{Equation 6-4}$$

$$\alpha = 0.02 \quad \text{Equation 6-5}$$

$$n = 42 \exp(-10.18w) + 5 \quad \text{Equation 6-6}$$

6.1.3 Failure criteria

A failure criterion for the material is assumed to follow Equation 6-7. This equation is plotted together with data taken from Sandén et al. (2017) This failure criteria is later used to determine if the material has cracked.

$$\sigma > 37777(\rho_d + 1425.2w - 1914.5) \quad \text{Equation 6-7}$$

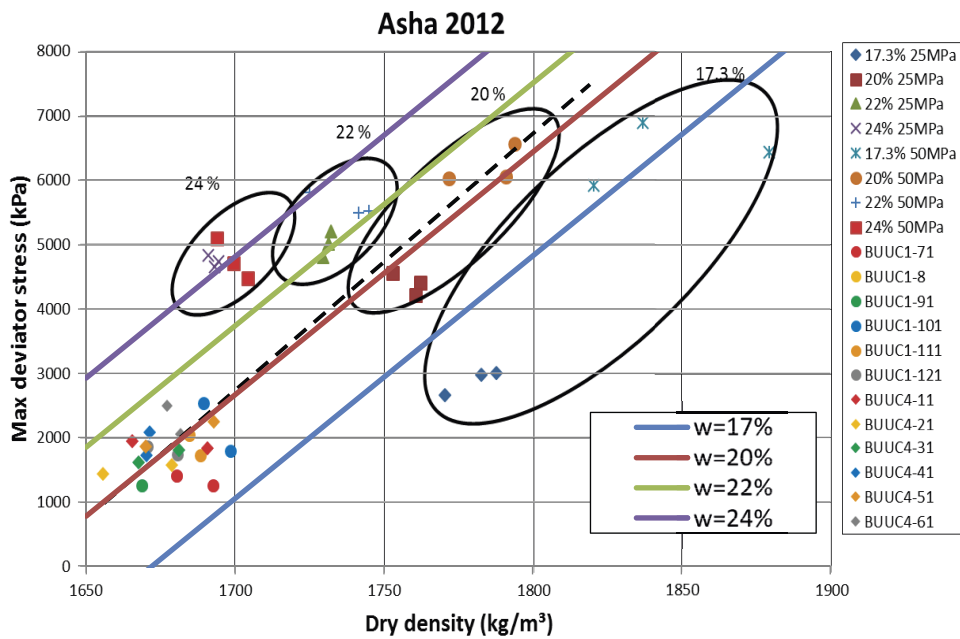


Figure 6-10. The failure criterion in Equation 6-6 compared to data from Sandén et al. (2020).

6.2 Swelling

The swelling process is modelled as a volumetric swelling similar to how a tangent coefficient of thermal expansion. But instead of having a swelling that is temperature dependent the swelling is dependent of water content. The swelling strain is calculated according to Equation 6-8.

$$\varepsilon_{sw} = \exp\left(\int_{w_{init}}^w \frac{1}{l(w)} \frac{dl(w)}{dw} dw\right) - 1 \quad \text{Equation 6-8}$$

Where l is the function of how length varies with water content. The approach here is to use measurements that were done in Eriksson (2017) and Svensson et al. (2019) to get an empirical expression how the bentonite is expanding when it absorbs water. Some data from MX-80 is shown in Figure 6-11.

Even though the shrinkage/expansion seem to be slightly higher in the compaction direction in this model it is assumed to be isotropic. The length change is fitted to empirical expression in Equation 6-9 and the volume is then the cube of the length expression. The first term in the expression describes the volume change during saturated conditions while the second term is added to describe the behaviour air starts to enter the material. In Equation 6-9 the ρ_f is a fitting density which is used to get the correct initial values on dry density, ρ_w is the density of water and ρ_s is the grain density

$$l(w) = \rho_f^{1/3} \left(\frac{1}{\rho_s} + w \frac{1}{\rho_w}\right)^{1/3} + \left(1 - \left(\frac{\rho_f}{\rho_s}\right)^{1/3}\right) \exp\left(-\frac{w \rho_f^{1/3} \rho_s^{2/3}}{3000 \left(1 - \left(\frac{\rho_f}{\rho_s}\right)^{1/3}\right)}\right) \quad \text{Equation 6-9}$$

The volume is not only affected by water content. The material will also be compacted by a mechanical pressure which will reduce the air-filled porosity. However, in this report only relatively dry material is considered and the modelled components are unconfined and therefore the pressures in the material are relatively small compared to the compaction pressures. This suggests that the volume changes due to mechanical pressure can be neglected and are therefore not added to the model used in this report.

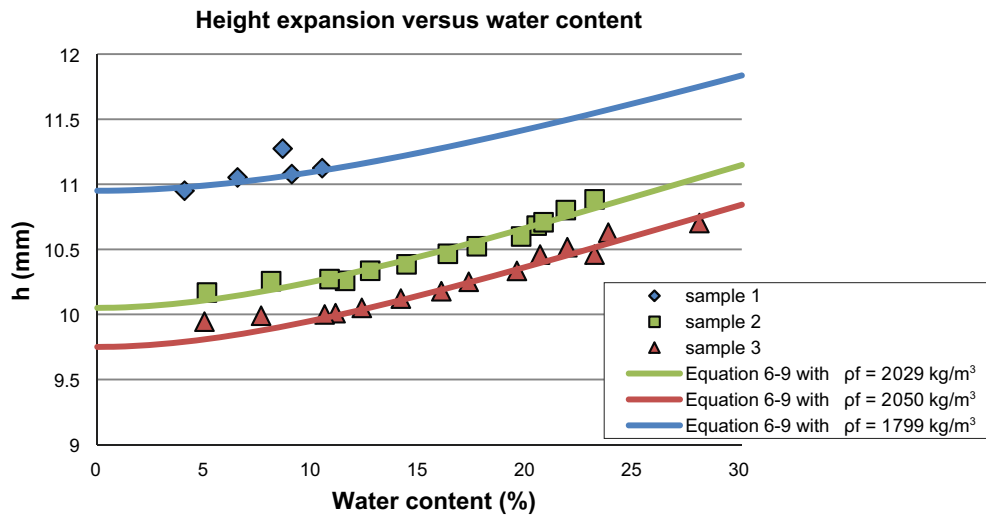


Figure 6-11. Measured dimension changes during shrinkage.

6.3 Coupling between hydraulics and mechanics

There is an obvious coupling between mechanics and hydraulics which is described in the previous chapter. The expansion/ shrinkage as well as the mechanical properties are affected by the water content which in turn affects the mechanical pressure. But there is also a coupling in the other direction, the suction of the material and therefore also the water content is affected by the mechanical pressure. The retention curve used in this report, for details see Eriksson (2019), is basically a function of the soil potential with is equal to the suction if no mechanical pressure is present. The relation between suction, soil potential and mechanical pressure can be described by Equation 6-10.

$$\Psi = p_s - p_m \quad \text{Equation 6-10}$$

Where p_s is suction and Ψ is the soil potential. The mechanical pressure, p_m , is positive when in compression. This expression can now replace the soil suction in the retention curve. This suggests that when the mechanical pressure is equal to the soil potential then the suction becomes zero. This two way coupling is very non-linear and therefore in this report a one way coupling is used. This can be done by assuming that the mechanical pressure is small compared to the soil suction which it should be if the material has relatively low water content. Also since most of the modelled cases can be considered to be unconfined the mechanical pressure should be low due to that the strength of the blocks limits this pressure. The initial suction is in the order of 50 MPa while the mechanical pressure is maximum around 1 MPa and therefore this simplification should not give to big deviations.

7 Test of the mechanical model

To test the model and how well it can describe the swelling during the installation phase the experiments in Chapter 3.3 is modelled. However only the test with an inflow of 0.001 l/min has been modelled because this test seem to be the most relevant.

Since the calculations have a quite high computational cost the following assumptions are made to simplify the calculations:

- **One way coupling**
The mechanical properties in the model are dependent on the hydraulics but in these models the suction is not dependent on the swelling pressure. This is assumed because the swelling pressure is expected to be low compared to the suction because the system is not confined
- **Pellet slot can be assumed to 2D**
This means that the water transport over the pellet slot will be infinite and thus should overestimate the water uptake in the buffer block.
- **No compaction of the material takes place**
The material has been compacted at 30–40 MPa no such pressures will be achieved in this calculations. At higher water contents were compaction could take place the bentonite is already close to saturation.

7.1 Boundary conditions and geometry

7.1.1 Geometry

The geometry consists a two bentonite blocks with an outer diameter of 1 650 mm and an inner diameter of 1 070 mm. The height of each block is 500 mm. see Figure 7-1. A steel plate with a thickness of 30 mm is placed on top of the block to simulate the weight used in the test.

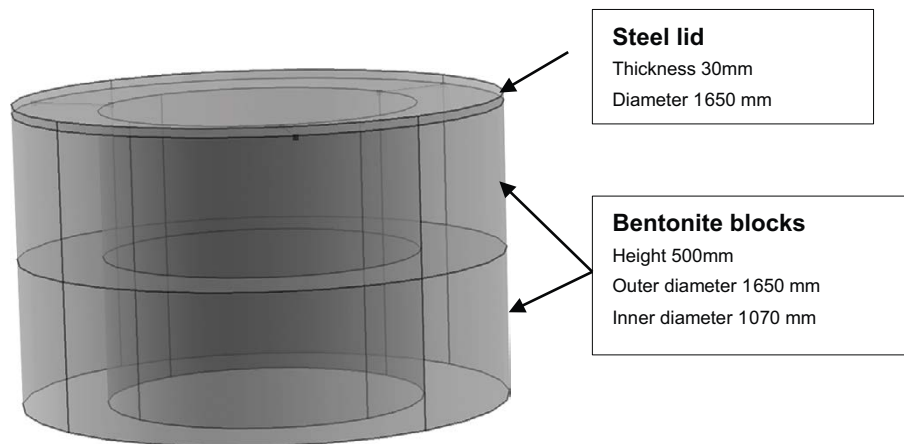


Figure 7-1. The geometry used in the model.

7.1.2 Hydraulic

The hydraulic boundaries are assumed to have no flow in the axial directions and at the inner diameter. The outer circumference a fixed pressure boundary condition is used. However, the pressure is a function of time and is taken from modelling of the pellet slot which is done in the same way as in Chapter 5. Figure 7-2, illustrates how the 2D result from the pellet slot modelling is projected on to the boundary of the 3D model. The transport model for the moisture in the block is basically the same as in Eriksson (2019). The initial water content is set to 17 % which correspond to a suction of approximately 66.7 MPa and the initial dry density is set to 1 707 kg/m³.

7.1.3 Mechanical

The mechanical boundaries are described in Figure 7-3. The lower surface of the block stack is considered to be fixed in z direction. The surface in-between the blocks and in-between the top block and the steel lid is modelled as a thin elastic layer. The reason for this is to allow the blocks to separate from each other. To make the behaviour more realistic this elastic layer is stiff in compaction but not in tension. The function for the spring force as a function of displacement is shown in Equation 7-1. All other surface is considered to be free. The material model used is described in Chapter 6. The initial condition is a stress free state.

$$p_{boundary} = 1000(1 - e^{-200000d}) Pa \quad \text{Equation 7-1}$$

d is the displacement of the thin elastic layer.

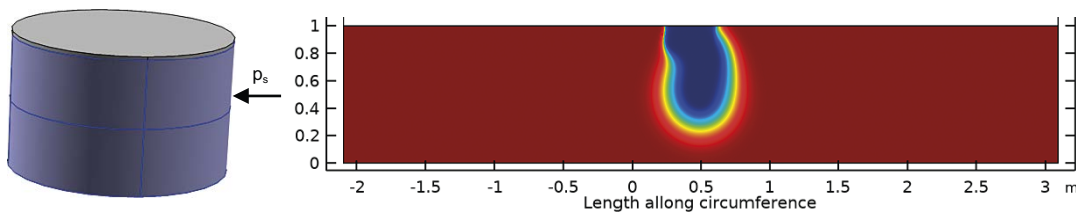


Figure 7-2. The geometry used in the model.

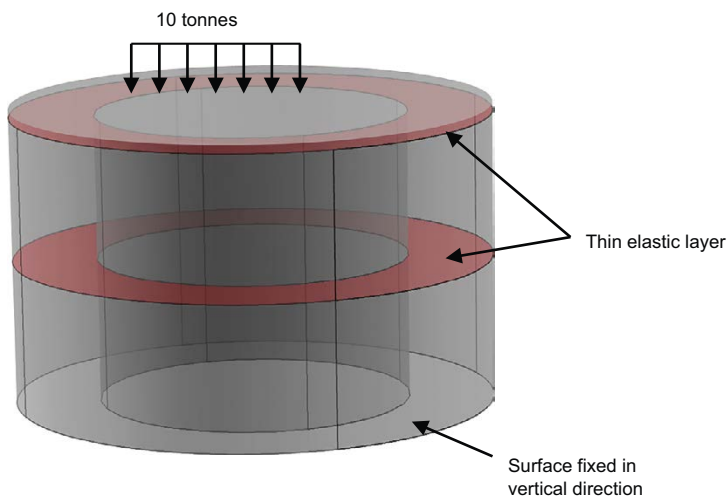


Figure 7-3. Mechanical boundaries.

7.2 Results

7.2.1 Swelling

The calculated swelling is large, approximately 3 times larger, compared to the test results, as can be seen in Figure 7-5. However, this might be explained by the fact that the blocks crack, see Chapter 7.2.2. In the model a large amount of the total swelling is due to that the slots in-between the blocks opens up, Figure 7-4. If no slots are assumed most of the swelling will be in radial direction because the yield strength of the relatively dry material towards the inner diameter is high. This would restrain the vertical swelling and force the swelling out towards the pellet slot. In this model the bentonite swells approximately 25 mm in radial direction, see Figure 7-6, which means that half of pellet slot has been taken up by the buffer blocks. This suggests that a radial swelling pressure on the outer boundary would start to develop which is not captured in the model. The model also has a more symmetric wetting then the test where the most of the water which distributed on the top surface went towards the direction of the 240 degree measuring point. This would explain why the 120 degree values are similar to the 240 degree values in the model but not in the test.

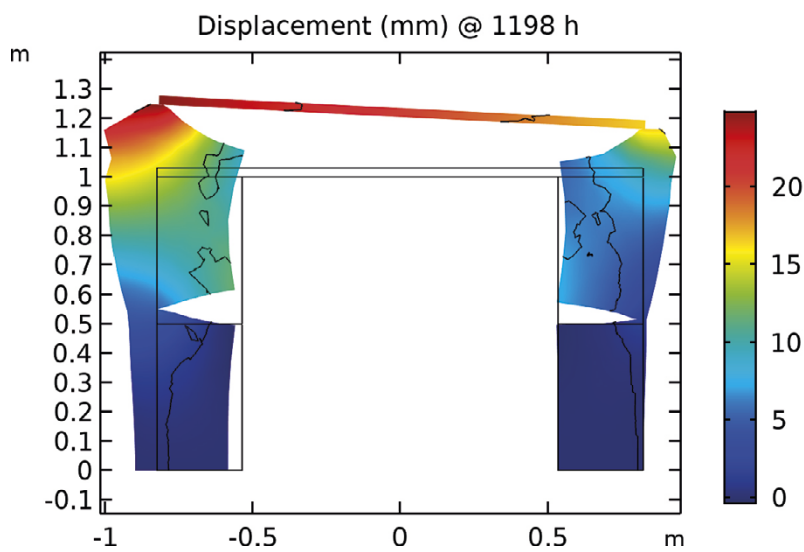


Figure 7-4. Cross section of the model showing the displacement in vertical direction in the 0° – 180° plane. All deformations are exaggerated 10 times. The black lines represent the surface where the failure criteria (Equation 6-7) is fulfilled. The inflow is located on the left side at 0.5 m height.

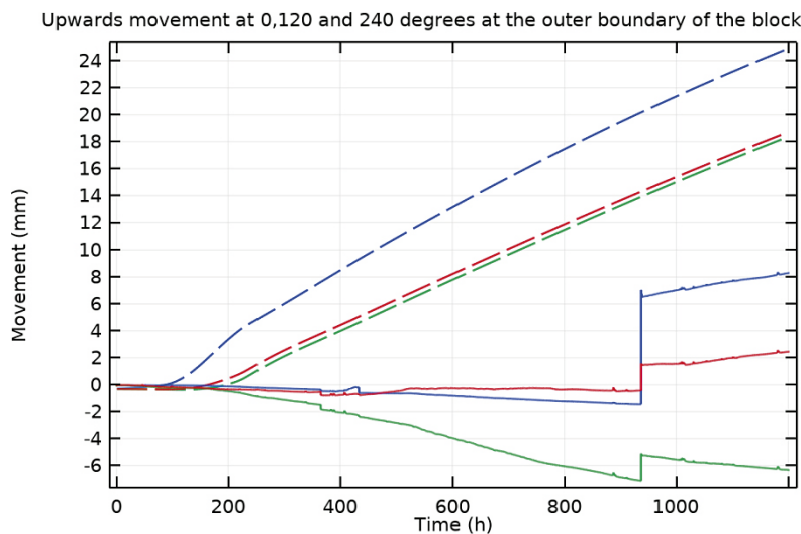


Figure 7-5. Comparison between test result of displacements (solid lines) and modelled (dashed lines). Blue lines is 0° , green lines is 120° and red lines 240° .

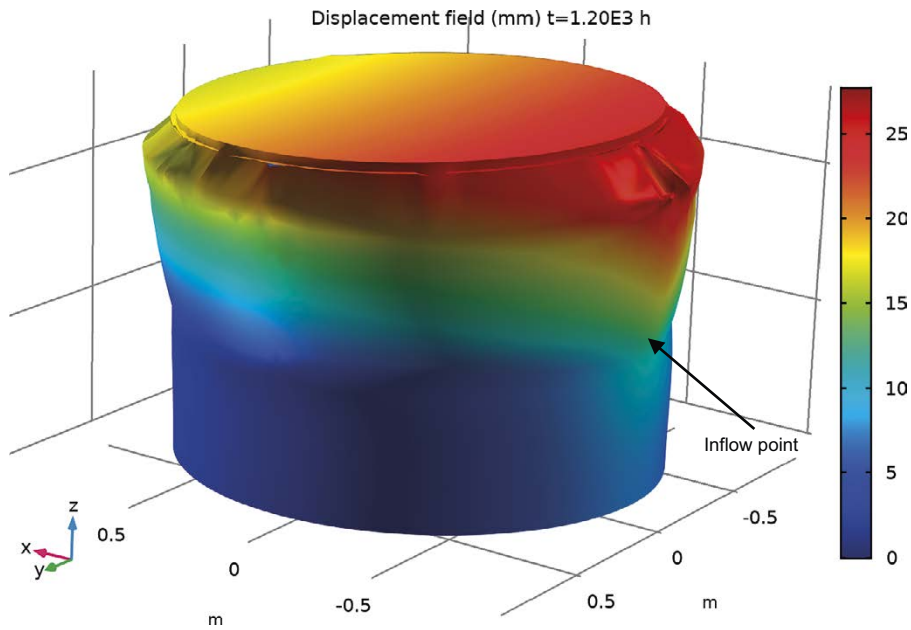


Figure 7-6. Displacement field after 1 200 hours.

7.2.2 Influence of cracking

Since the swelling in the model is so much higher than in the test the influence of cracking of the blocks will also be examined a little more in detail and how this could affect the result. If the failure criteria in Chapter 6.1.3 are used, volumes in the model which have experienced stresses large enough to create cracks can be identified. In Figure 7-7 the areas where the failure criteria have been fulfilled are shown in red. From the comparison with the test it can be seen that cracked areas seem to be similar in the model and in the test. The model also predicts that the upper block is cracked all the way through the block while the lower block is not. This is the same behaviour that was seen in the test. In Figure 7-8 it can be seen how the area where the failure criteria have been fulfilled develops with time.

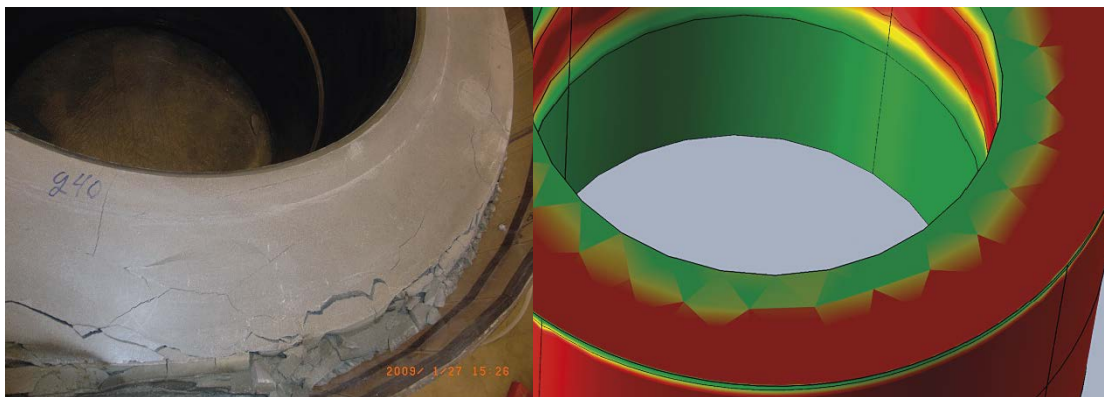


Figure 7-7. Cracks in the top block after the test compared to the volume where the failure criterion has been fulfilled (red areas in the right figure).

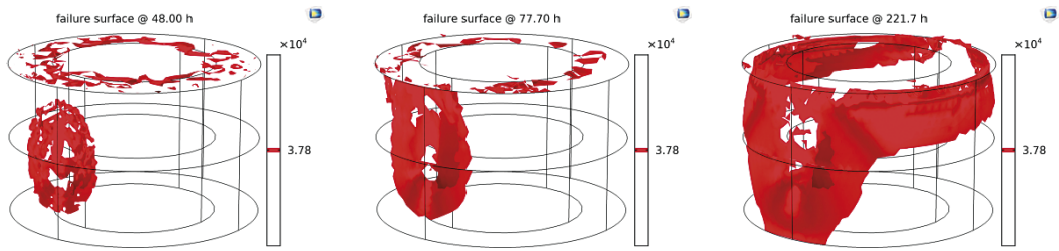


Figure 7-8. Time development of the failure surface from the model.

Since the model seems to be able to predict areas that will crack an attempt to compensate the upwards swelling for this cracking. Therefore it is assumed that the area that has been cracked has no structural strength and can therefore not keep supporting the weight of the extra weight on top of the blocks. This is done by calculating the most inner point of the block where the failure criterion has not been fulfilled, see Figure 7-9, and calculate the displacement in that point. The material which is considered cracked is assumed to fall in to the pellet slot. The result of this calculation is shown in Figure 7-10 together with the test result and the modelling result from Chapter 7.2.1. The result of this calculation gives values much closer to test values.

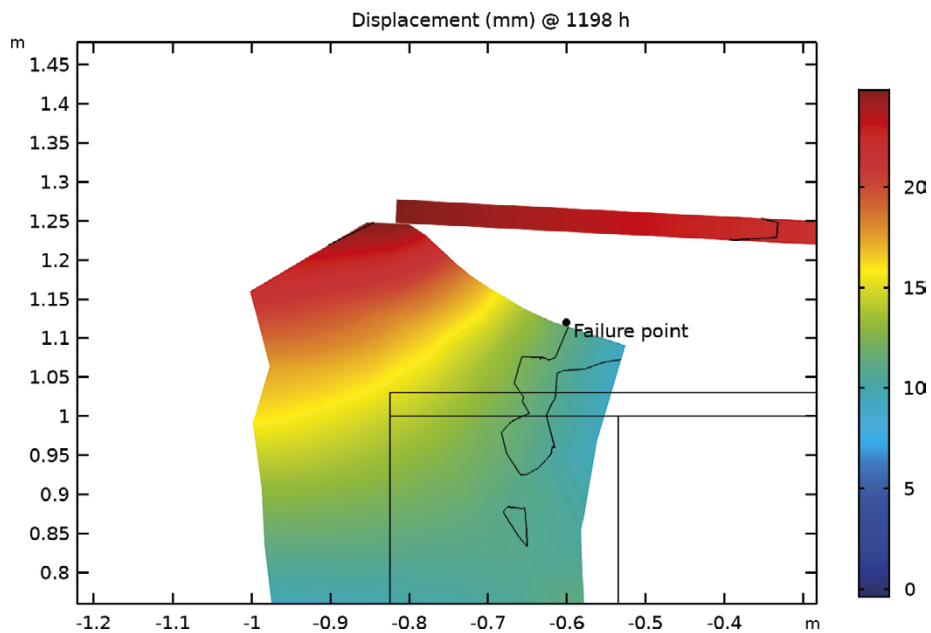


Figure 7-9. Showing the load bearing point which moves with time, in this figure the time is 1 200 hours.

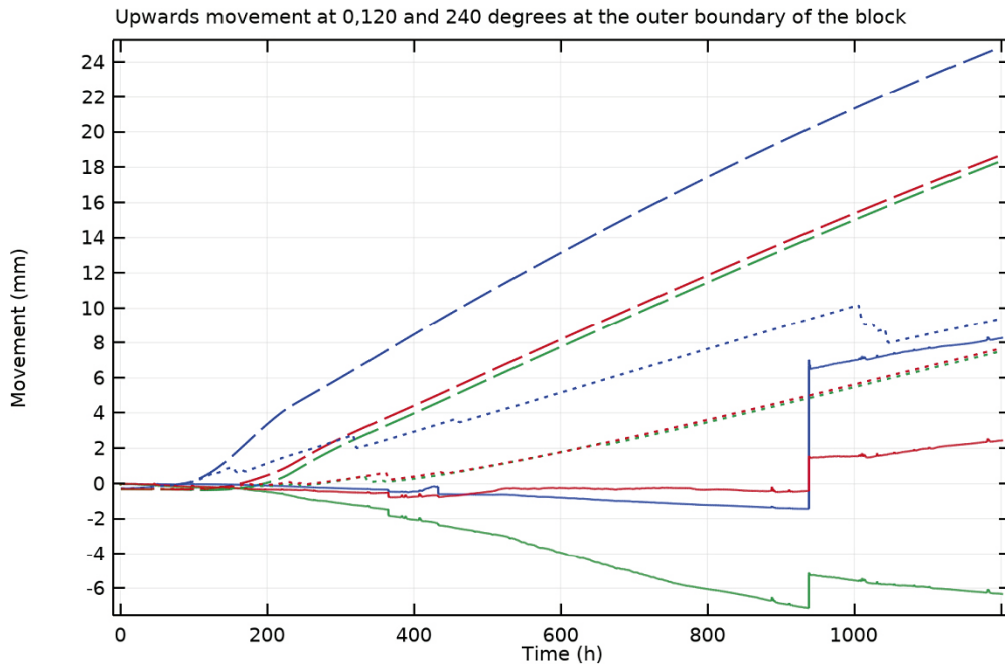


Figure 7-10. Showing the displacement of the top surface in three points. Blue line at 0 degrees (inflow), green line at 120 degrees and red at 240 degree. The solid lines is the test, dashed lines are the model without cracking and dotted lines are the model with cracking.

7.2.3 Validity of the assumption of one way coupling

To test if the assumption using a one way coupling and removing the swelling pressures effect on the hydraulic properties is valid the swelling pressure divided with the suction is plotted in Figure 7-11. The result shows the swelling pressure is less than 25 % in basically the whole model. This suggests that the model might overestimate the water uptake in the block slightly due to the fact that the swelling pressure effect on the retention curve is not considered. However, it seems that this effect is not that large and that the approach of removing the suction dependence on swelling pressure is acceptable in this case. In the top part of the block the suction is approximately 0.8 MPa and the swelling pressure is 200 kPa after 1200 h.

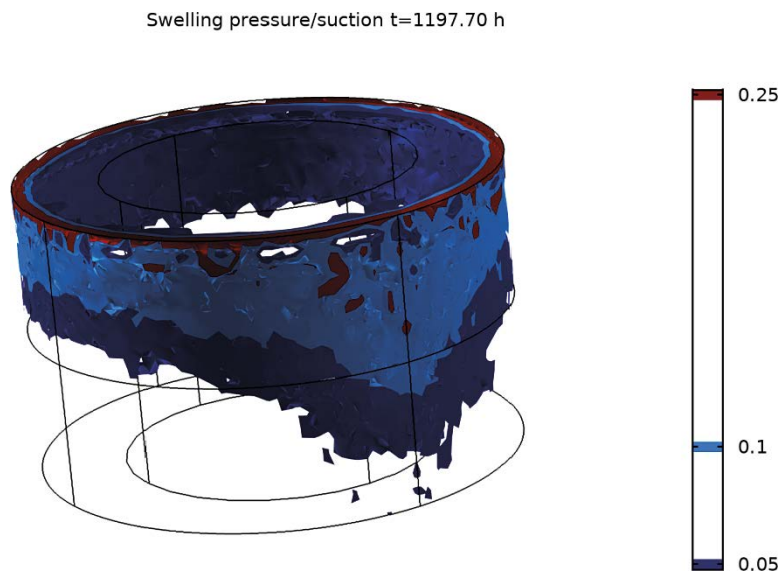


Figure 7-11. Swelling pressure divided with the suction at time approximately 1200 h. The plot suggest that the model is underestimating the suction with less than 10 % in most of the volume and at maximum 25 %.

8 Conclusions

Models have been developed that can predict the swelling with different wetting patterns during the initial phase after the buffer has been installed. However the models are advanced and need to consider a lot of processes like slots in-between the blocks, cracking of the blocks and how the water flows in pellet fillings.

The model for water transport in pellet fillings seem to work very well and the key to getting a good result seems to be to include a piping model. The model can replicate results from a wide range of water inflows. In this report 10^{-5} l/min to 0.1 l/min has been tested with good results. The addition of a piping model should make it possible to also include an erosion model for the channels if needed. It should also be possible to model the pellet filling in the backfill. However, then the model must probably be done in 3D which would require some more development.

The mechanical model is in quite early stage of development the result seems promising. However, the material model is currently based on relatively small amount of data in quite a small range why updates to the model might be needed.

Although the models have a high computational cost they should be able to scale up to model a full deposition hole if some optimization work is done. This could then help to determine the limit between a wet hole, where buffer and backfill needs to be installed after each other, and a dry deposition hole, where all the buffer can be installed first before backfilling starts.

References

SKB's (Svensk Kärnbränslehantering AB) publications can be found at www.skb.com/publications.

Andersson L, Sandén T, 2012. Optimization of backfill pellet properties. Åskar DP2. Laboratory tests. SKB R-12-18, Svensk Kärnbränslehantering AB.

Börgesson L, Sandén T, Dueck A, Andersson L, Jensen V, Nilsson U, Olsson S, Åkesson M, Kristensson O, Svensson S, 2015. Consequences of water inflow and early water uptake in deposition holes, EVA project. SKB TR-14-22, Svensk Kärnbränslehantering AB.

Eriksson P, 2017. Compaction properties of bentonite clay. SKB TR-16-16, Svensk Kärnbränslehantering AB.

Eriksson P, 2019. Development of thermo-hydraulic model for pellet fillings. SKB P-19-12, Svensk Kärnbränslehantering AB.

Lundgren C, Johannesson L-E, 2020. Optimering av buffertpellets för KBS-3. Laboratorieförsök på fyra olika pellets. SKB R-19-25, Svensk Kärnbränslehantering AB. (In Swedish.)

Luterkort D, Johannesson L-E, Eriksson P, 2017. Buffer design and installation method. Installation report. SKB TR-17-06, Svensk Kärnbränslehantering AB.

Nord M, Eriksson P, Johannesson L-E, Frizell A, 2020. Full-scale buffer installation test. Test of the behaviour of a segmented buffer during the installation phase. SKB TR-20-16, Svensk Kärnbränslehantering AB.

Sandén T, Börgesson L, 2010. Early effects of water inflow into a deposition hole. Laboratory test results. SKB R-10-70, Svensk Kärnbränslehantering AB.

Sandén T, Börgesson L, Nilsson U, Dueck A, 2017. Full scale Buffer Swelling Test at dry backfill conditions in Äspö HRL. In situ test and related laboratory tests. SKB TR-16-07 Svensk Kärnbränslehantering AB.

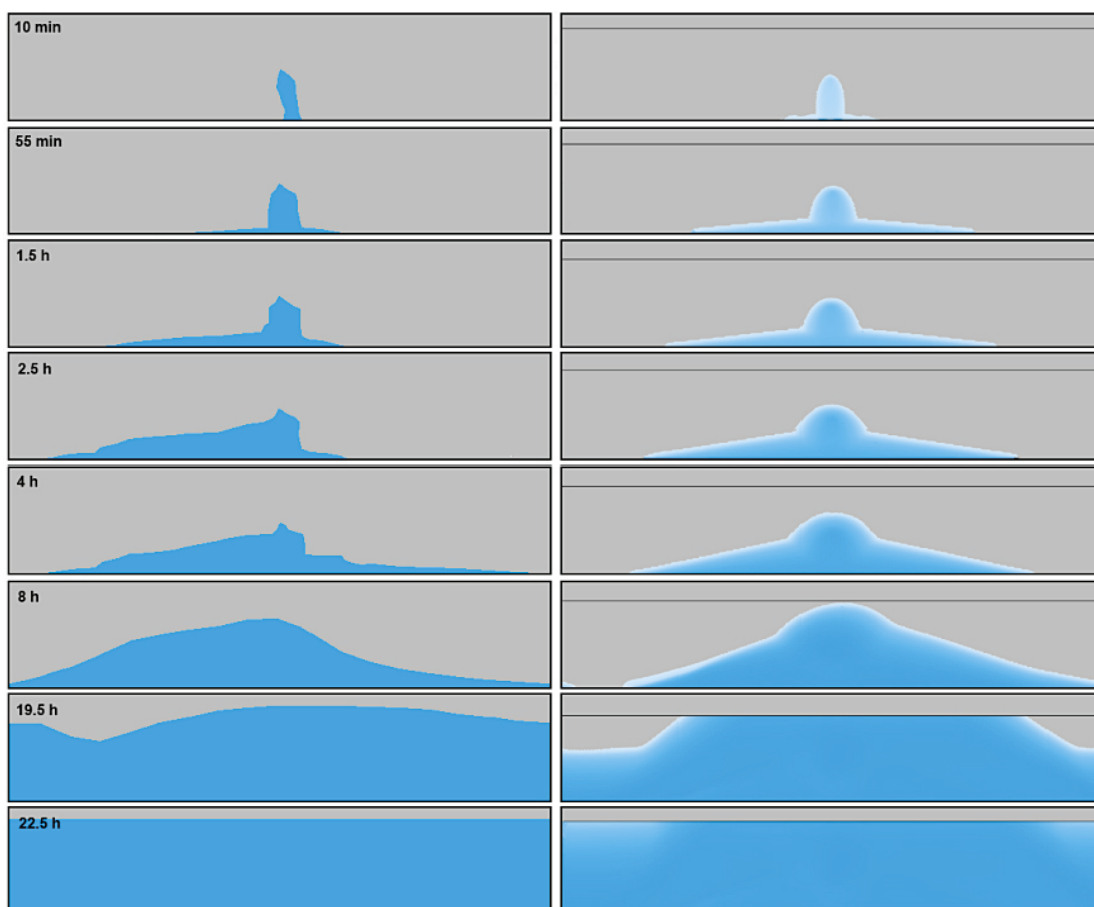
Sandén T, Jensen V, 2017. Pellet optimization – influence of fine material. KBP1011 Water handling during backfill installation. SKB R-16-15, Svensk Kärnbränslehantering AB.

Sandén T, Kristensson O, Lönnqvist M, Börgesson L, Nilsson U, Goudarzi R, 2020. Buffer swelling. Laboratory tests and modelling. SKB TR-20-04, Svensk Kärnbränslehantering AB.

Svensson D, Eriksson P, Johannesson L-E, Lundgren C, Bladström T, 2019. Development and testing of methods suitable for quality control of bentonite as KBS-3 buffer and backfill. SKB TR-19-25, Svensk Kärnbränslehantering AB.

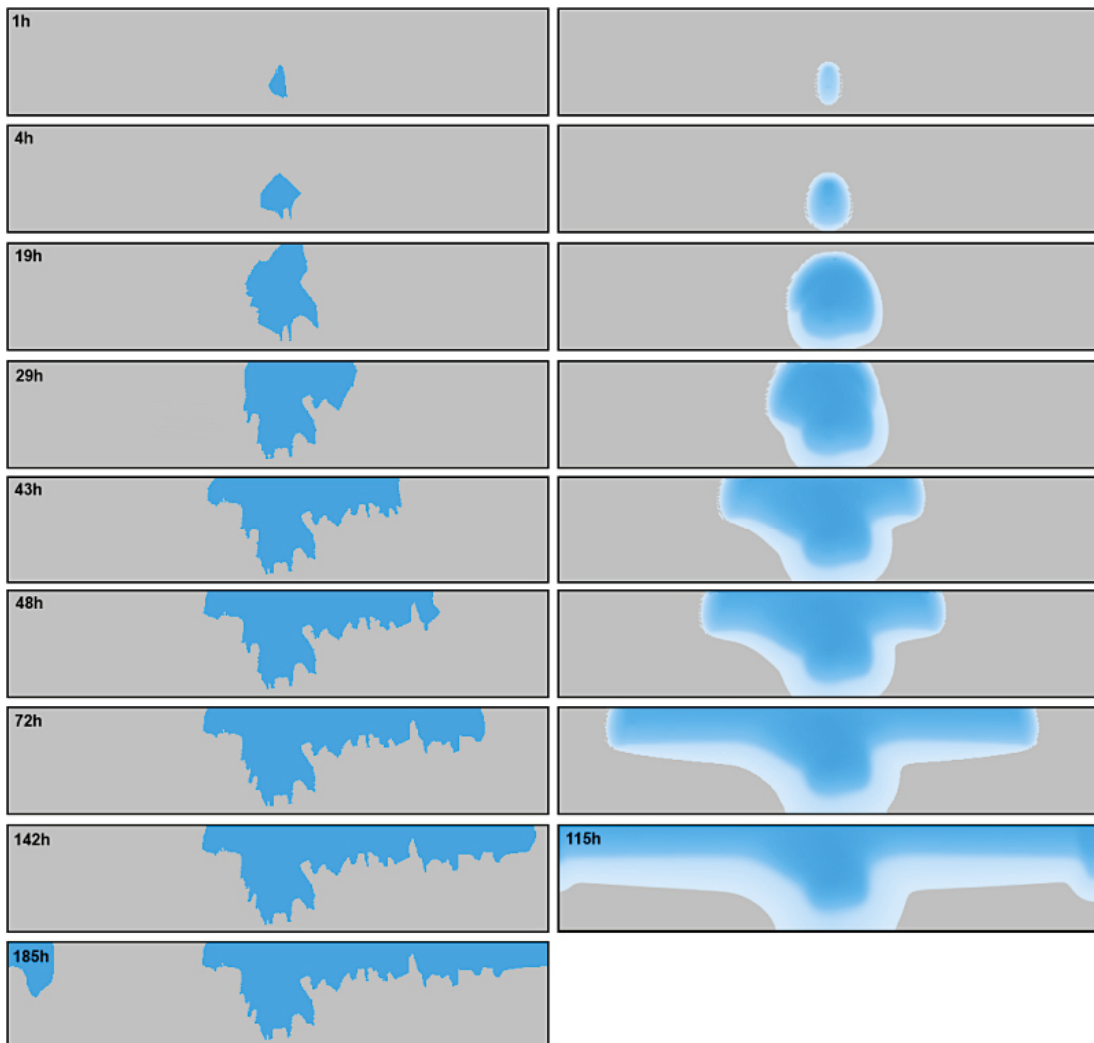
Åberg A, 2009. Effects of water inflow on the buffer – an experimental study. SKB R-09-29, Svensk Kärnbränslehantering AB.

Comparison of modelled wetting pattern and measured, 0.1 l/min



Data from the test, to the left, for different times compared to the modelling results, to the right, for the same times.

Comparison of modelled wetting pattern and measured, 0.01 l/min



Data from the test, to the left, for different times compared to the modelling results, to the right, for the same times if nothing else is stated. The main difference at longer times I likely to that the test was drained but not the model. The model was stopped at 115 h due to that the surface was sealed and water transport is only suction driven.

Derivation of boundary condition for the channel

To calculate what flow will exit perpendicular to the channel an analogy with ohms law is used.

$$U = R * I$$

From this the following can be identified

$$U = -\frac{dp}{dx}$$

$$I = Q$$

$$R = \frac{\mu}{\kappa}$$

Then an assumption that the pressure gradient is constant in the whole channel is made. This should be a valid assumption because the inflow I proportional against the pressure gradient but the power of the system is proportional to the square of the pressure gradient. This means that if there is any variation in the pressure gradient in the channel then the power of the system should increase. However, all system strive to minimize their energy, therefore it should be valid to assume that the pressure gradient is constant along the channel. In the case we let water exit in discrete points then the system will look like Figure A3-1.

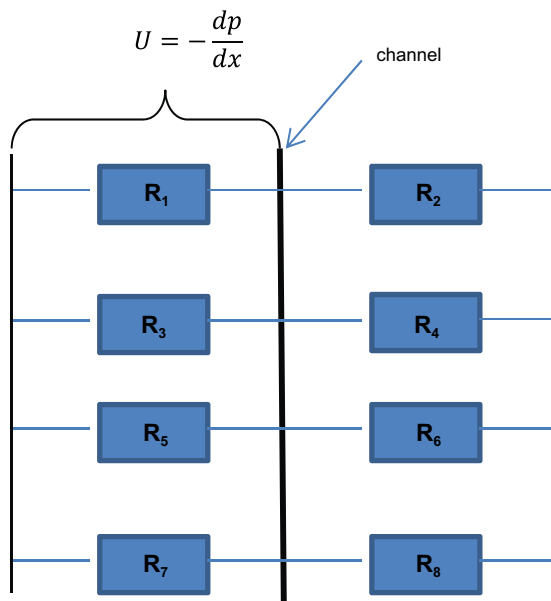


Figure A3-1. Representation of the system flow can exit the channel in discrete points.

The total flow resistant can then be calculated with the following equation:

$$\frac{1}{R_{tot}} = \sum_{i=1}^n \frac{1}{R_i}$$

By adding reducing the distance between each point we can make this to a continuum according the following equation.

$$\frac{1}{R_{tot}} = \int_0^L \frac{\kappa(l)}{\mu} dl$$

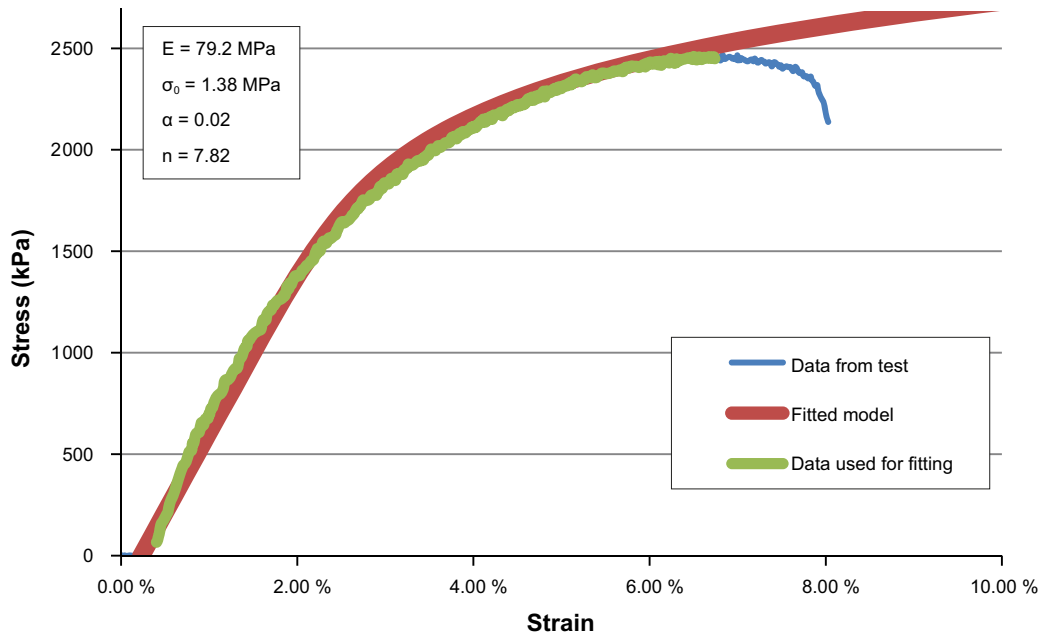
Where l is the coordinate in the channels length direction, x is the direction perpendicular to the channel and L is the total length of the channel. The flow in each point, $Q(l)$, can then be calculated through:

$$Q_{tot}R_{tot} = Q(l)R(l) = Q(l) \frac{\mu}{\kappa(l)}$$

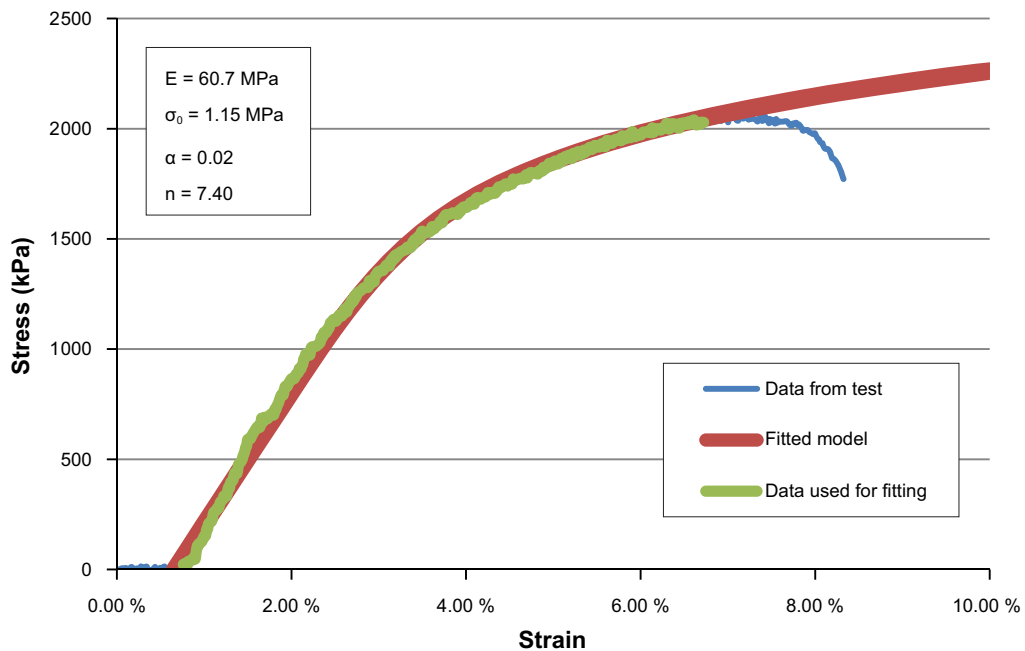
This can be rewritten to:

$$Q(l) = \frac{Q_{tot}\kappa(l)}{\mu \int_0^L \frac{\kappa(l)}{\mu} dl}$$

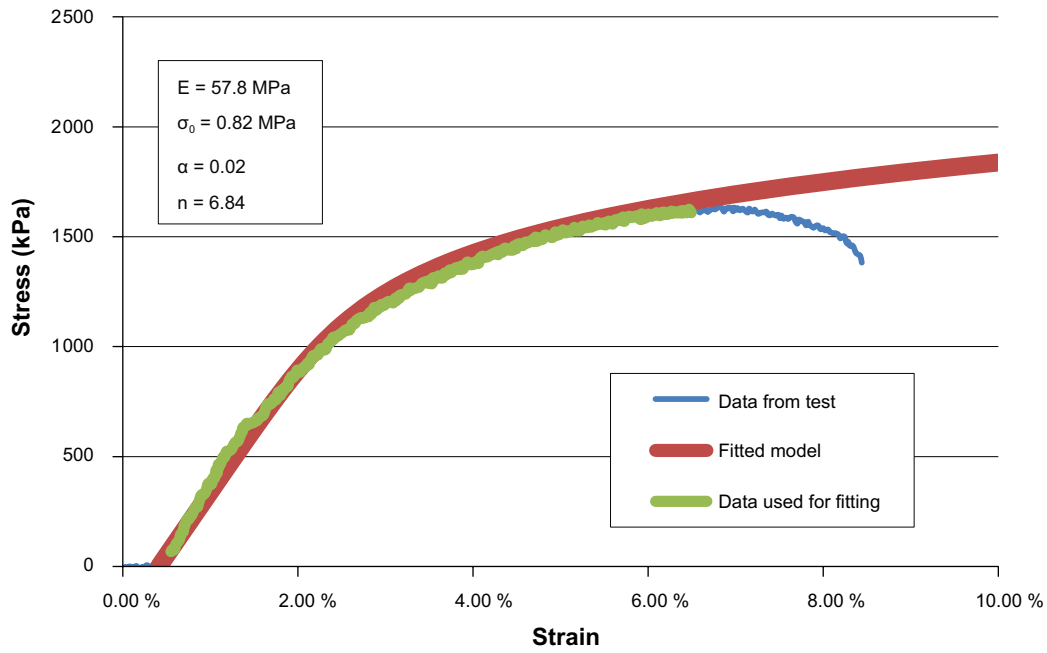
Data from uniaxial compression test on saturated samples of MX-80



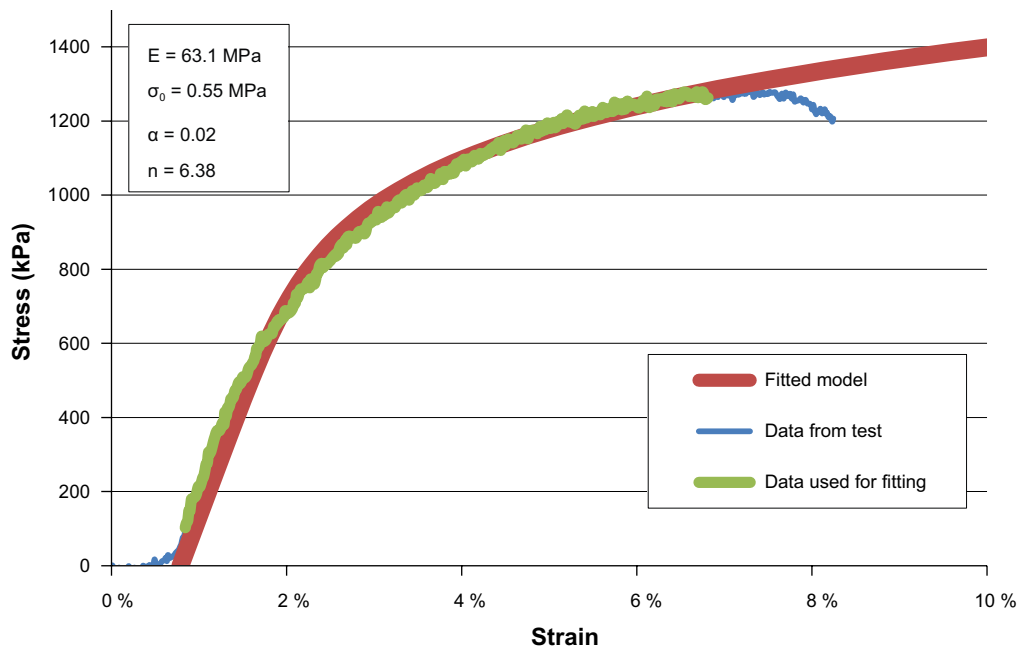
Saturated sample with water content 26.7 %.



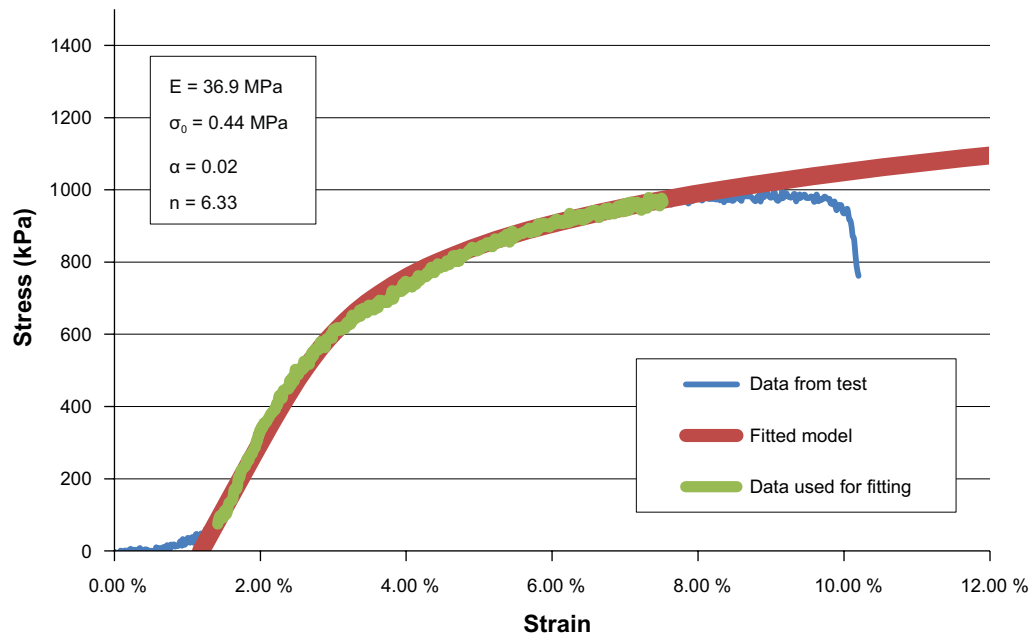
Saturated sample with water content 28.6 %.



Saturated sample with water content 30.2 %.

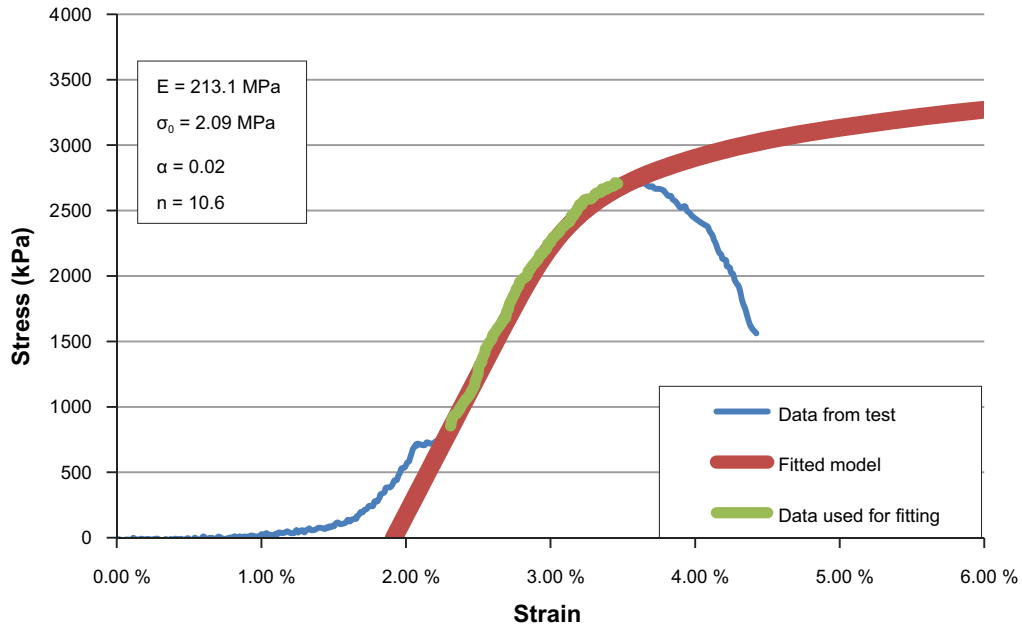


Saturated sample with water content 32.7 %.

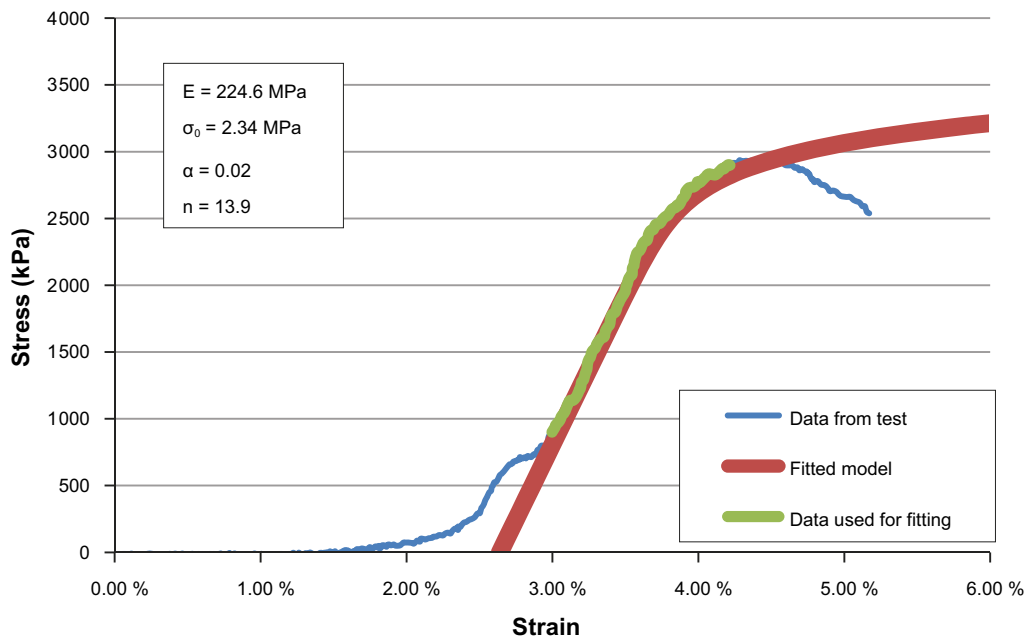


Saturated sample with water content 34.7 %.

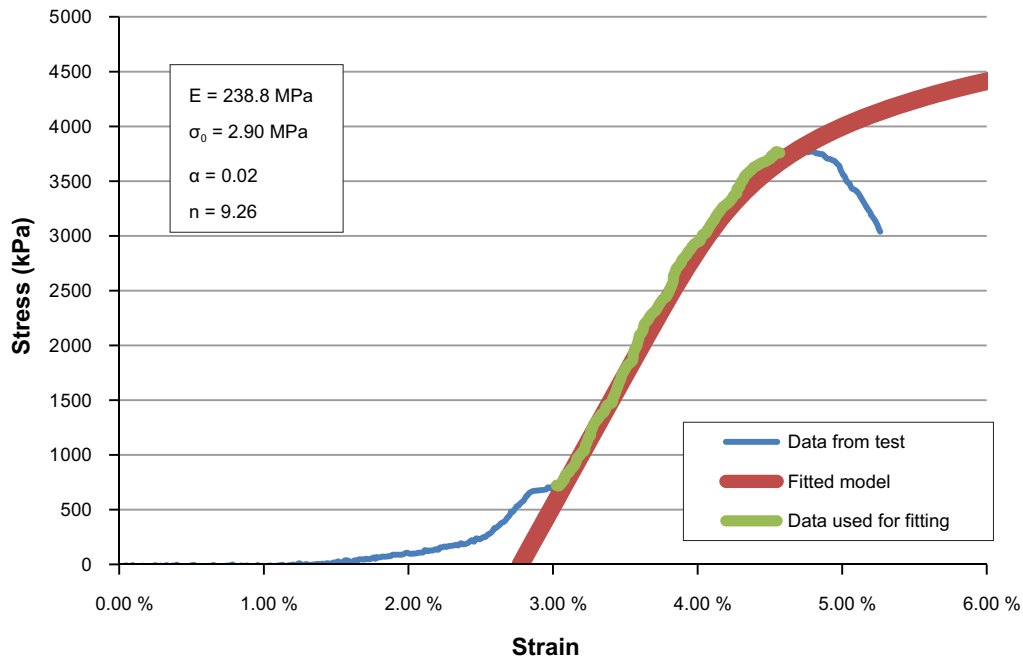
Data from uniaxial compression test on unsaturated samples of Bara-Kade 1002



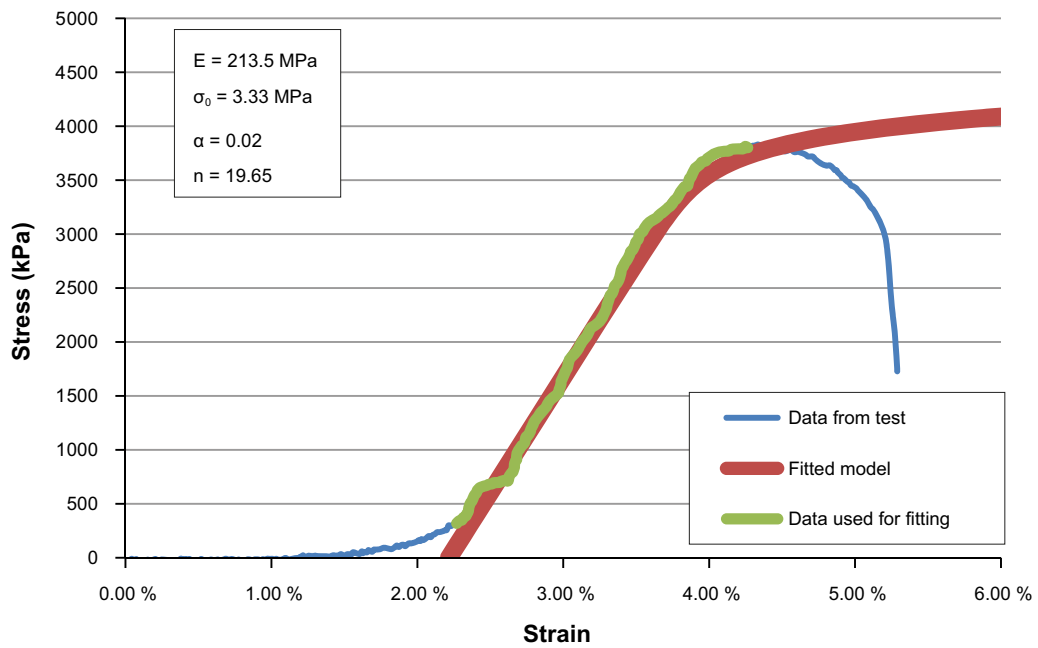
Sample 1. Water content 16.4 % and dry density 1 685 kg/m³.



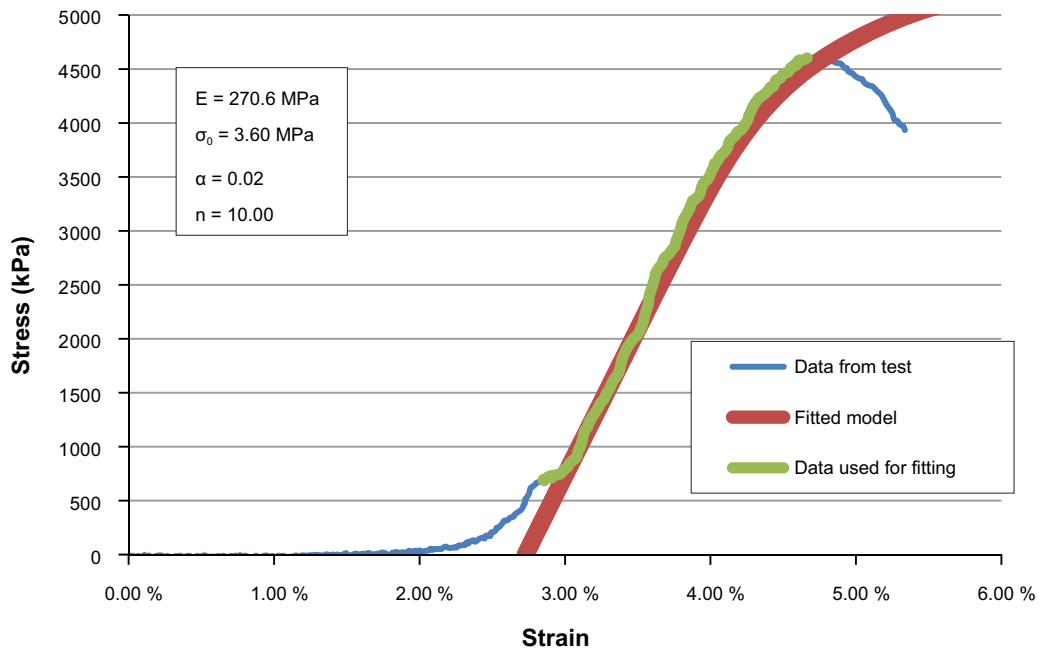
Sample 2. Water content 16.3 % and dry density 1 699 kg/m³.



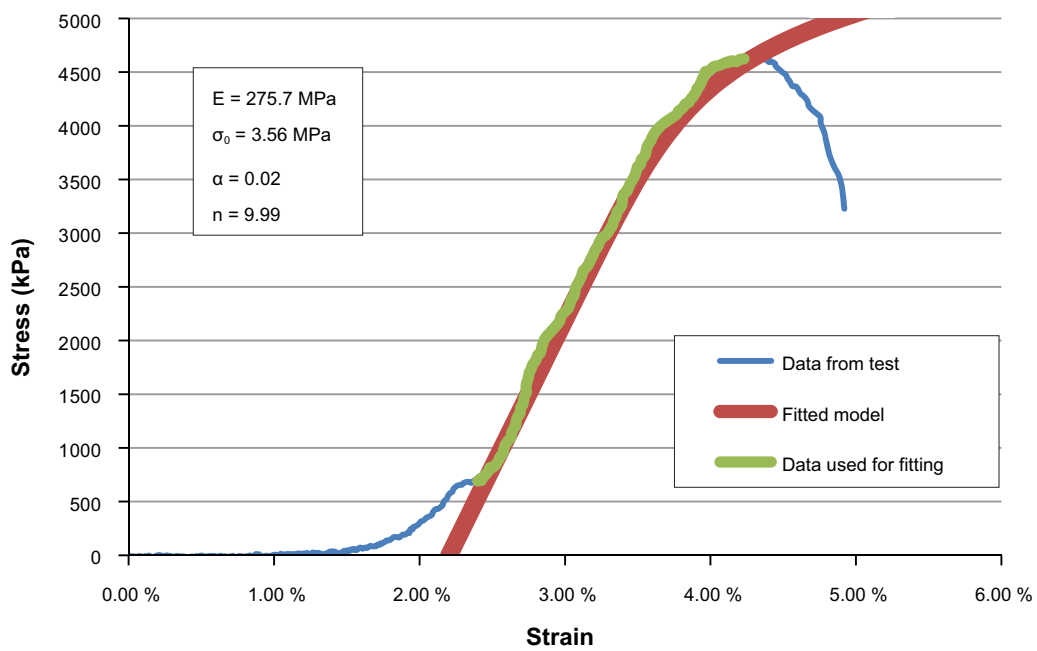
Sample 3. Water content 16.4 % and dry density 1 705 kg/m³.



Sample 4. Water content 16.1 % and dry density 1 714 kg/m³.



Sample 5. Water content 16.3 % and dry density 1 730 kg/m³.



Sample 6. Water content 16.2 % and dry density 1 749 kg/m³.

SKB is responsible for managing spent nuclear fuel and radioactive waste produced by the Swedish nuclear power plants such that man and the environment are protected in the near and distant future.

skb.se